I-7992758 c.2
CPUB

Energy, Mines and Resources Canada | Energie, Mines et Ressources Canada

CANMET

Canada Centre for Mineral and Energy Technology | Centre canadien de la technologie des minéraux et de l'énergie

CHARACTERIZATION OF LONG-LIVED RADIOACTIVE DUST CLOUDS GENERATED IN URANIUM MILL OPERATIONS

J. BIGU AND P. DUPORT

ELLIOT LAKE LABORATORY

JANUARY 1987

This report is prepared for the Atomic Energy Control Board under Financial Encumbrance AECB FE 85/4.

MINING RESEARCH LABORATORIES
DIVISION REPORT MRL 87-105(TR)

1-7992758 c.2
CPUB

CHARACTERIZATION OF LONG-LIVED RADIOACTIVE DUST CLOUDS GENERATED IN URANIUM MILL OPERATIONS

by

J. Bigu* and P. Duport**

ABSTRACT

The characteristics of long-lived radioactive dust clouds generated in several mechanical and physico-chemical operations in a uranium mill have been investigated. The study consisted of the determination of dust size distribution, and of the size distribution of radionuclides associated with particulate matter in the size range <0.1 to 26 μm. Experiments were conducted using several cascade impactors operating at different sampling flow rates. Two different types of cascade impactors were used. Radionuclide identification was done using α-spectrometry and γ-spectrometry. Long-lived and short-lived radionuclides were identified in dust samples. The characteristics of the dust clouds depended on the mill operation. The following operations were studied: crushing (vibrating grizzly, jaw crusher, cone crusher); screening; ore transportation; grinding; acid leaching; counter-current decantation; yellowcake precipitation and drying; and yellowcake packaging. In addition, other dust and radioactivity measurements have been carried out.

Keywords: Long-lived radioactive dust; Uranium; Mine mill; Dust; Radioactivity.

*Research Scientist and Radiation/Respirable Dust/Ventilation Project Leader,
**Scientific Advisor, Atomic Energy Control Board (AECB), Ottawa, Ontario.

CANMET LIBRARY
3 2329 00056884 5
c.2
CPUB

CARACTÉRISATION DES NUAGES DE POUSSIÈRE RADIOACTIFS À LONGUE PÉRIODE RÉSULTANT DES PROCÉDÉS MÉCANIQUES ET PHYSIO-CHIMIQUES DE BROYAGE

par

J. Bigu* et P. Duport**

RÉSUMÉ

Les caractéristiques des nuages de poussière radioactifs à longue période qui se forment pendant les procédés mécaniques et physico-chimiques de broyage de l'uranium ont fait l'objet d'une étude. Celle-ci avait pour but de déterminer la distribution granulométrique des radionucléides inhérents aux particules dont les dimensions variaient de <0.1 à 26 µm. Plusieurs impacteurs à cascade à débits différents ont été mis à l'essai. Deux impacteurs à cascade de type différent ont été utilisés. Les radionucléides ont été identifiés au moyen de la spectrométrie α et de la spectrométrie γ. Les radionucléides à longue vie et les radionucléides à courte vie que contenaient les échantillons de poussière ont été identifiés. Les caractéristiques des nuages de poussière sont reliées aux procédés de broyage. Les procédés suivants ont fait l'objet d'une étude : le concassage (crible à barres vibrant, concasseur à mâchoires, broyeur à boulets); le criblage; le transport du minerai; le broyage; la lixiviation acide, la décantation à contre-courant; la concentration d'oxyde jaune d'uranium et le séchage; et la manutention de l'oxyde jaune d'uranium. D'autres mesures de la poussière et de la radioactivité ont également été effectuées.

Mot clé : Poussière radioactive à longue période; Uranium; Poussière; Radioactivité.

*Chercheur scientifique et Chef de projet Radiation, Poussière inhalable, Ventilation.

**Conseiller scientifique, Commission de contrôle de l'énergie atomique (CCEA), OTTAWA (Ontario).

CONTENTS

	Page
ABSTRACT	i
RÉSUMÉ	ii
INTRODUCTION	1
EXPERIMENTAL APPARATUS AND METHODS	2
MECHANICAL OPERATIONS	5
EXPERIMENTAL RESULTS AND DISCUSSION	7
SUMMARY AND CONCLUSIONS	22
ACKNOWLEDGEMENTS	23
REFERENCES	23

TABLES

No.		
1.	Cascade impactors operating characteristics	25
2.	Cascade impactors data for several mechanical operations in a uranium mill	26
3.	Cascade impactors data for several physico-chemical operations in a uranium mill	27
4.	Average values of MMAD and AMAD for different mill operations...	28
5.	Alpha-particle energy corresponding to some members of the uranium and thorium natural radioactive chains	29
6.	Gamma-energy (main peak) of some of the radioisotopes identified in dust samples from several mill operations	30
7.	Total and respirable dust concentration during some milling mechanical operations	31
8.	Working Level measured by a WLM-300 continuous Working Level Monitor at several locations	32
9.	Radon progeny grab-sampling data by Thomas-Tsivoglou method at several locations	33

FIGURES

1.	Block diagram of mechanical and physico-chemical operations in a uranium mill	34
2.	Alpha-particle spectra corresponding to different mill operations	35
3.	Percentage cumulative dust versus EAD for the 'grizzly' fragmentation operation	36
4.	Percentage cumulative dust versus EAD for the jaw crusher operation	37

5. Percentage cumulative dust versus EAD for the cone crusher operation 38

6. Percentage cumulative dust versus EAD for screening operations . 39

7. Percentage cumulative dust versus EAD for the fine ore bin/conveyor belt 40

8. Percentage cumulative dust versus EAD for the yellowcake packaging operation 41

9. Percentage cumulative LLRD and radon progeny alpha-activity versus EAD for the 'grizzly' fragmentation operation 42

10. Percentage cumulative LLRD and radon progeny alpha-activity versus EAD for the jaw crusher 43

11. Percentage cumulative LLRD alpha-activity versus EAD for the cone crusher 44

12. Percentage cumulative LLRD and radon progeny alpha-activity versus EAD for the screening operations 45

13. Percentage cumulative dust and percentage cumulative LLRD alpha-activity versus EAD for the fine ore bin/conveyor belt operation 46

14. Percentage cumulative LLRD and radon progeny alpha-activity versus EAD for the fine ore bin/conveyor belt operation 47

15. Percentage cumulative LLRD and radon progeny alpha-activity versus EAD for the grinding operation 48

16. Percentage cumulative LLRD alpha-activity versus EAD for the grinding operation 49

17. Percentage cumulative LLRD alpha-activity versus EAD for the yellowcake packaging operation 50

18. Percentage cumulative dust, and percentage cumulative LLRD, and radon progeny alpha-activity versus EAD for acid leaching 51

19. Percentage cumulative dust, and percentage cumulative LLRD, and radon progeny alpha-activity versus EAD for acid leaching 52

20. Percentage cumulative LLRD, and radon progeny alpha-activity versus EAD for counter-current decantation operations 53

21. Percentage cumulative LLRD and radon progeny alpha-activity versus EAD for counter-current decantation operations 54

22. Percentage cumulative dust, and percentage cumulative LLRD (AMAD), and radon progeny alpha-activity versus EAD for counter-current decantation operations 55

23. Percentage cumulative dust (MMAD) versus EAD, and percentage cumulative LLRD (AMAD) and radon progeny alpha-activity versus EAD for solvent extraction 56

24. Percentage cumulative LLRD and radon progeny alpha-activity versus EAD for solvent extraction 57

25. Percentage cumulative dust (MMAD) versus EAD, and percentage cumulative LLRD (AMAD), and radon progeny alpha-activity versus EAD for yellowcake precipitation 58

26. Percentage cumulative dust (MMAD) and LLRD (AMAD) alpha-activity versus EAD for yellowcake precipitation during the drying phase 59

27. Percentage cumulative LLRD and radon progeny alpha-activity versus EAD for yellowcake precipitation 60

28. Percentage cumulative LLRD and radon progeny alpha-activity versus EAD for yellowcake precipitation 61

29. Percentage cumulative LLRD alpha-activity versus EAD for yellowcake precipitation 62

30. Dust concentration for several physico-chemical operations 63

31. Radon progeny Working Level versus time for several physico-chemical operations 64

INTRODUCTION

Inhalation of airborne radionuclides poses a potential health hazard to occupational workers in the nuclear industry. For this reason, monitoring of radioactivity concentration levels for dose exposure calculation purposes is a subject of considerable practical interest.

Some concern has recently been expressed with regards to the inhalation of respirable dust (1-10 μm size range) containing long-lived radioisotopes, as once inhaled and lodged in the respiratory system they will remain active as long as they are not eliminated by natural biological processes.

There is sparse information available regarding the long-term health effects of worker's exposure to long-lived radioactive dust (LLRD) such as that produced in underground uranium mine and uranium mill operations, nor is much data available on either LLRD chemical make-up or size distributions in uranium mines and mills. This information is important to identify the main radioisotopes in LLRD, their concentration in air, and their size distribution as the latter determines the LLRD deposition characteristics in the respiratory system (1-3).

This report presents experimental data collected in a uranium mill. Long-lived radioactive dust is generated in the course of mechanical and physico-chemical unit operations carried out in the separation and refining processes of uranium, or uranium chemical compounds, from uranium ores.

The data in this report pertain to the main mechanical and physico-chemical milling operations. These include the following operations: ore transportation by conveyor belts, crushing, grinding, screening (i.e., sizing), acid leaching, counter-current decantation (CCD), solvent extraction, yellowcake precipitation, yellowcake drying and yellowcake packaging.

Measurements were conducted of LLRD and radon progeny associated with

dust in the 1-30 μm size range, and radon progeny in the submicron size range. A variety of other dust and radioactivity measurements were also carried out. This study was suggested by Atomic Energy Control Board (AECB) and was conducted under partial funding from the same organization.

EXPERIMENTAL APPARATUS AND METHODS

Size distribution analyses of radioactive dust, radioactive aerosol and dust were conducted by means of two 10-stage, radial slot-design, cascade impactors, model 210, manufactured by Sierra Instruments Inc. (U.S.A.), now Anderson. Depending on the particular application, the cascade impactors were operated with either 10 stages or 8 stages. In the latter case, the cascade impactors were operated with the last two ultrafine impactor stages removed. These two stages were eliminated at the expense of losing some size distribution information, but with the obvious benefit of substantially increasing the amount of dust collected on the remaining eight impactor stages.

Glass Fiber filters (47 mm diameter), with radial slot design similar to that of the cascade impactor stages, were used as substrates to collect the samples. The cascade impactors were operated for about 12 hours at a time at a sampling flow-rate of 10.5 L/min (8-stage), and 3.3 L/min (10-stage).

The Glass Fiber substrates placed behind the stages of the cascade impactors enabled determination of the size distribution (mass median aerodynamic diameter (MMAD), and geometric standard deviation) of dust by determining the weight of the filters before and after the sampling period. The substrates were dried before and after sampling to eliminate moisture. Ambient temperature and pressure were carefully noted during sampling and results were corrected according to standard operating procedures. Total dust (mass concentration and activity concentration) was also estimated from

cascade impactor data.

Radioactivity (α-particle) measurements on the impactor substrates also enabled calculation of the long-lived radioactive dust (LLRD), and radon progeny, size distribution, i.e., activity median aerodynamic diameter (AMAD), and geometric standard deviation.

Also used in the determination of LLRD and radon progeny size distribution were two small, 8-stage, personal Marple cascade impactors (4). These impactors differ significantly from the Sierra impactors in a number of ways such as size, weight and geometry. The Marple impactors are much smaller and lighter than the Sierra impactors. The impactor stages slot design is also different, i.e., six radial slots for the Marple impactor as opposed to four radial slots for the Sierra impactors. The Marple impactors were operated at a nominal flow-rate of 2 L/min. Stainless steel substrates were used as dust collectors. Because of the low flow rate at which these impactors are operated and the relatively large weight of the substrates, as compared with Glass Fiber filters, no attempt was made to measure dust, only the radioactivity associated with it.

The total LLRD and radon progeny concentrations were also estimated from impactor data. Radon progeny were measured 40 min after sampling. A counting time of 5 min was chosen. The α-particle activity of the LLRD was measured 1-2 weeks after sampling to allow the radon progeny and thoron progeny, if any, to decay away completely. Because of the low LLRD activity, each sample was counted several times for 30 min each time, and the average value, after subtracting the background, was used in the calculations.

The procedure used for the determination of dust, activity, and size distribution from the cascade impactor data was as follows:

1. Activity (dpm, i.e., disintegrations per min) and dust mass collected on each impactor stage were carefully noted.

2. Total activity and total dust mass from all the stages of the impactor, including the backfilter (BF), were measured.
3. Percentage (%) activity and % dust mass for each impactor stage were calculated.
4. Cumulative % of dust mass and cumulative % of activity, less than $D_{p,50}$ (see below), were estimated as follows. Dust mass (or activity) % of the BF was used as cumulative % for the last ultrafine stage. The cumulative % for the next stage was obtained by adding the % of dust mass (or activity) to the cumulative % dust mass (or activity) corresponding to the previous stage, and so on.
5. Cumulative % dust mass (or activity), less than $D_{p,50}$, versus EAD was plotted.

The variable $D_{p,50}$ is defined as the particle cut-off at 50% collection efficiency for spherical particles of density one. The magnitude EAD is the Equivalent Aerodynamic Diameter defined as the size of a spherical particle of density 1 g/cm^3 which has the same terminal settling velocity as the sampled particle.

In addition to cascade impactors, total dust mass in the respirable size range from ~1 μm to ~10 μm was monitored with a continuous, optical system, dust sampler model Mini-Ram PDM-3, manufactured by GCA (U.S.A.). Furthermore, respirable dust was measured using nylon cyclone samplers (cut-off size 3.5 μm). Total dust was determined by open-face filter techniques.

Identification of long-lived radionuclides was done using α- and γ-spectrometry of several dust samples. Spectrometric analyses were carried out using a silicon-barrier detector (SiBD) spectrometer for α-spectrometry, and a high purity Germanium detector (HPGD) for γ-spectrometry.

Radon progeny Working Levels, WL, were measured for several operations using a continuous Working Level monitor model WLM-300 (EDA Instruments,

Toronto), and by grab-sampling using the Thomas-Tsivoglou method. Radon gas concentrations were measured by grab-sampling using the scintillation cell method.

Dust generated by mechanical and physico-chemical operations in a uranium mill was sampled at several transfer points and locations in the mill. A brief description of the mechanical and physico-chemical operations of the mill are given below.

MECHANICAL OPERATIONS

Uranium ore from an ore pit and a nearby uranium mine was dumped by a truck loader into a piston-type rock breaker, i.e., 'vibrating grizzly', where the ore was broken into smaller sizes and dropped into a chute which fed a conveyor belt. Ore smaller than a given size was shaken directly into the chute. Sampling was done at the grizzly/conveyor belt transfer point which will be denoted hereafter as transfer point 1 (TP1).

Crushed ore from the grizzly was transferred to a jaw-crusher via a vibrating screen where finer ore drops through by-passing the second crushing operation. Coarser ore is further crushed to a smaller size by the jaw-crusher. Ore passing through the vibrating screen and the crusher is transported by a conveyor belt to special screens for size selection. Sampling in this area was done below the jaw-crusher feeding point, but above the transfer point onto the conveyor belt. This location will be denoted hereafter as transfer point 2 (TP2).

Ore from the jaw-crusher operation was fed onto a set of screens where the fines passed directly through to a conveyor belt and were stored in fine ore bins ready for grinding. The coarser ore was fed into a cone-crusher. Sampling was conducted in an area adjacent to the screens at the same level. This will be denoted as transfer point 3 (TP3).

Ore from the screens was further reduced in size by the cone-crusher and fed to a conveyor belt which was routed back to the screening operation. Sampling was carried out at the base of the cone-crusher, below and away from the feed point. This sampling location will be referred to as transfer point 4 (TP4).

Ore from the cone-crusher/screen system was delivered to the top of fine ore bins, for storage, by a 150 m long conveyor belt. The ore was then fed from the base of the fine ore bins to the grinder for further ore size reduction. Sampling was done at the end of the long conveyor belt on top of the fine ore bins. This sampling location will be referred to as transfer point 5 (TP5).

Uranium ore was reduced to its final size by means of grinding with steel balls and cylinders. Sampling was conducted beside the grinder, i.e., transfer point 6 (TP6).

From the grinder onward the ore underwent a number of physico-chemical operations before its final processed stage in the mill, i.e., as yellowcake, and subsequent packaging in the packaging plant.

Several physico-chemical operations in the mill were monitored. Broadly speaking, this part of the mill circuit is as follows. The ground uranium ore from the rod and ball mills is treated with a neutral thickener. The neutral thickened slurry is treated with sulphuric acid, sodium chlorate and steam (acid leaching), and the leached slurry is directed to a series of counter-current decantation (CCD) tanks where the tailings are removed from the solution as a 55% solid slurry. Counter-current decant of the liquid solution, containing the uranium-rich phase, is fed to a clarification plant where the solution is passed through several sand filters to remove any suspended solid matter. The clarified liquid solution is directed to a liquid-liquid extraction plant. The effluent from the CCD is neutralized with

milk of lime and removed from the plant to a tailings pond.

The filtered/clarified uranium-compound liquid phase solution is treated with a mixture of kerosene, alcohol and an amine. Kerosene is used as a liquid carrier. The alcohol is employed to keep the amine dispersed in the liquid phase. The amine reacts chemically with the uranium compound and forms an organic complex which is subsequently stripped from the liquid solution by means of sodium chloride. The scrubbed raffinate is treated with milk of lime as indicated above.

The high grade uranium compound solution from the extraction process is treated with milk of magnesia where the uranium compound is precipitated as yellowcake. The yellowcake solution is thickened by settling and water evaporation. The yellowcake is dried in a dryer, stored in a yellowcake storage bin, and finally packaged in special drums in the yellowcake drying and packaging section for shipping and further processing and purification in the fuel fabrication cycle.

Monitoring was carried out on the following physico-chemical operations: acid-leaching, counter-current decantation, solvent extraction, and yellowcake precipitation and drying. The last mill operation, a mechanical operation, i.e., yellowcake packaging, was also monitored. Sampling at this location will be referred to as transfer point 7 (TP7). (It should be noted that the terminology 'transfer point' is only applied here to mechanical operations.)

Figure 1 shows a flow diagram of the mill where measurements were carried out. The flow diagram includes mechanical and physico-chemical operations.

EXPERIMENTAL RESULTS AND DISCUSSION

Measurements were conducted during March and June 1986. Four cascade

impactors were used, namely: the two Sierra impactors labelled EMR and C, and two 8-stage Marple impactors labelled M_1 and M_2 or simply M. During March, the EMR and C impactors were operated with 10-stages and 8-stages, respectively. During June, the two Sierra impactors were operated with 8-stages. Furthermore, the two Sierra impactors were located side by side at each sampling station during the March measurements. The purpose was twofold: to determine if the number of stages would affect the MMAD and AMAD, and to obtain two samples in the same location for statistical purposes.

Because of the low sampling flow-rate of the Marple impactors, and the relatively low dust concentration in mill air at the time, no attempt was made to determine the dust mass on the different stages. Hence, no MMAD data from these impactors are available. Marple impactors were only used to gather radioactivity data to calculate the AMADs and the LLRD concentration in air.

Table 1 shows the average operating characteristics of the cascade impactors used. The table shows the operating sampling flow-rates and the corresponding cut-off sizes for each stage. The size range covered with these instruments was from about 0.06 μm to approximately 26 μm, depending on the number of stages and flow rates used.

The data obtained with the cascade impactors have been summarized in Tables 2 to 4. and Figures 3 to 29. Figure 2 shows α-spectra for some samples.

Tables 2 and 3 show cascade impactors data for long-lived radioactive dust and radon progeny. The data included are MMAD, AMAD, geometric standard deviations, dust concentration, LLRD concentration, and the specific radioactivity associated with dust. Tables 2 and 3 show the following features of practical interest:

1. The AMAD corresponding to the LLRD is, on average, larger than the corresponding MMAD of the carrier dust;

2. The MMAD decreases as the ore is crushed, screened and ground in the different mechanical operations in the mill. The MMAD follows the natural sequence of fragmentation from the vibrating grizzly to the grinding operations. The approximate range of values for the MMAD was 3 to 15 μm.
3. As for the MMAD, the values for the AMAD (LLRD) depended on the type of mechanical operation. The range of values found was approximately 3.7 to 19 μm.
4. The MMAD and AMAD corresponding to the last mechanical operation, in fact the last mill operation, namely, yellowcake packaging, were between the values corresponding to the vibrating grizzly and the jaw crusher.
5. Significant differences in the values of the MMAD were found in samples taken at the same location with impactors operated with different number of stages and air flows (12% to >50%). The same applies to the AMAD. There is no satisfactory explanation for the large discrepancy found between the EMR and M_2 impactors data collected during the grinding operation. However, the data corresponding to the EMR impactor are presumed to be more consistent with this milling operation.
6. As expected, the AMAD corresponding to the radon progeny associated with dust was much less than its corresponding MMAD. The AMAD obtained was in the range 0.15 to 0.7 μm, indicating that the radon progeny are preferentially associated with submicron particulate matter. The reader should be cautioned regarding the use of cascade impactors for radon progeny size distribution analysis for the reasons given below.

   The size of particles carrying radon progeny ranges from ~0.005 μm to ~0.2 μm. The number of radon progeny atoms borne by particles larger than 0.2 to 0.3 μm is negligible compared to the total number of aerosol particles. The small dimension of these particles makes them highly

susceptible to collection by diffusion as well as by impaction in cascade impactors. This phenomenon increases as the diameter decreases and makes the measurement of radon progeny size by cascade impactors difficult to interpret.

Measurement of fine particles ($\lesssim$0.3 μm) by cascade impactors is rather complex because of the difficulty in differentiating the contribution in the number of particles (or activity) collected on different stages by impaction from that due to diffusion. This is particularly true when the activity is the variable measured. When mass (or mass distribution) is the variable measured, biases introduced by the unwanted diffusion collection of fine particles is undetected on stages with a cut-off diameter larger than 0.5 μm because the mass of a particle varies with the cube of the diameter. The bias from fine particles would only be detected when the concentration is very high compared to that of larger particles (mixtures of mineral dust and diesel smoke for example)(see also reference 5).

7. No satisfactory explanation can be found at present for some significant differences in dust concentration measured in high dust-production areas of the mill by the EMR and C cascade impactors placed side by side (see Table 2). It should be noted that the dust concentration ratio between the C and EMR impactors is $\lesssim$2.0, whereas the ratio for their respective sampling flow-rates is about 3.2.
8. For the physico-chemical operations (see Table 3), the largest values for AMAD and MMAD were found in the counter-current decantation (CCD), and yellowcake precipitation operations. Acid leaching and solvent extraction has lower values for the above variables, particularly solvent extraction.
9. As expected, the LLRD activity concentration was by far the highest for

the yellowcake packaging operation followed by yellowcake precipitation. Comparison of other mill operations is somewhat difficult because of the different air dilution factors between March and June. It should be noted that measurements of the mechanical operations were preferentially conducted during March, whereas monitoring of physico-chemical operations was carried out in June. For the mechanical operations, the highest LLRD concentration was found for yellowcake packaging (1.3×10^5 mBq/m^3) followed by crushing by the vibrating grizzly (1570 mBq/m^3). For the physico-chemical operations the highest LLRD concentration was obtained for the yellowcake precipitation followed by counter-current decantation and acid leaching (2110, 394, 252 mBq/m^3, respectively).

10. Total dust mass concentration ranged widely depending on the mill (mechanical) operations. It was highest at the vibrating grizzly and for the yellowcake packaging operations ($\geq$6 mg/m^3) followed by the jaw crusher ($\geq$1.5 mg/m^3). Dust concentration for the physico-chemical operations was lower than for the mechanical operation. Solvent extraction showed the lowest dust concentration.
11. Significant differences in the values of the AMAD were found in samples taken with the Sierra and Marple impactors. However, there are insufficient experimental data to quantify this statement unambiguously, and more work under controlled experimental conditions is necessary to compare the performance of the two types of impactors.
12. Radioactivity measurements of the dust collected on cascade impactor substrates show that gross α-activity was not always linearly proportional to the amount of dust collected on the impactors substrates It was found that the ratio of α-activity to dust mass decreased as the latter increased. These results suggest significant α-particle absorption in dust. From these data it may be concluded that although

relatively high dust mass is preferable to low dust mass for MMAD calculations, this may lead to substantial uncertainties in the determination of the AMAD. As discussed later, the actual α-activity measured on each stage should be verified by liquid scintillation counting of the same samples, or by neutron activation analysis.

It is presumed that the contribution to the LLRD concentration (mBq/m^3) and its specific concentration (mBq/mg), from some cascade impactor stages, may have been underestimated for mill operations that generated substantial amounts of dust. Self-absorption problems can be minimized by choosing sampling times to ensure that adequate amounts of dust will be collected for accurate MMAD determination, while at the same time consistent with low α-particle absorption necessary for reliable measurements of the AMAD. It should be noted that during March dust concentrations were much higher than in June when doors and windows remained open day and night.

It should be noted that the specific activity for the yellowcake precipitation operation calculated from data obtained in March and June differed by a factor of 10 to 14. This large difference can be attributed to differences in the grade of processed ore, and to 'cleaner' practices during June, e.g., open doors and the like. The former supposition was later confirmed by mill personnel, i.e., the grade of the ore processed in June was much lower than the grade processed in March. Notice, that the specific activities for the two experimental runs on March were quite close and within experimental error. The same applies to the two runs in June, with somewhat larger differences. These data indicate that the grade of the ore was constant for each case, e.g., March and June, although much higher for March.

Table 4 shows average values of MMAD and AMAD calculated from data in Tables 2 and 3 for the mill operations investigated.

Figures 3 to 29 show data for MMAD and/or AMAD for all mill operations. Figures 3 to 17 refer to mechanical operations whereas Figures 18 to 29 correspond to physico-chemical operations. The data shown by these Figures complement and/or support the data discussed in Tables 2 to 4.

Figures 3 to 8 show the cumulative dust mass percentage of size less than $D_{p,50}$ versus $D_{p,50}$, from mechanical operation samples taken with the two Sierra cascade impactors, EMR and C, at several transfer points, i.e., locations in the mill. As indicated above, the MMAD calculated from these data, for the two cascade impactors, differed somewhat in some cases, although the two instruments were located side by side, and hence sampling took place under practically identical conditions.

Figures 9 to 15 and Figure 17 show the cumulative LLRD α-particle activity percentage associated with dust of size less than $D_{p,50}$ versus $D_{p,50}$, for the Sierra impactors. Also shown in Figures 9, 10, 12, 14, 15 and 17 is the cumulative short-lived α-particle activity percentage associated with particulate matter of size less than $D_{p,50}$ versus $D_{p,50}$, for the same impactors. The short-lived α-particle activity referred to above corresponds to the radon progeny associated with particulate matter of size less than 1 μm. As for the MMAD case, AMAD for the LLRD and radon progeny differed somewhat for the two cascade impactors (see also reference 5).

Figure 16 shows the cumulative LLRD activity percentage associated with dust of size less than $D_{p,50}$ versus $D_{p,50}$, for an 8-stage Marple cascade impactor (grinding operation). The graphs show the uncorrected and corrected results. Data were corrected to take into account the different dust deposition efficiency in each impactor stage. The clearly curve-shaped graphs obtained for the uncorrected and corrected data are not clearly understood, but they seem to consist of two straight lines, i.e., log-normal, distributions meeting at $D_{p,50} \sim 6$ μm. The α-particle activity/dust size

distribution obtained with the Marple impactor is quite different from the distribution obtained with the Sierra impactors. Although the shape of the graphs obtained with the Marple impactor cannot satisfactorily be explained at present, it is consistent with other measurements carried out in the mill during the monitoring of some physico-chemical operations as reported below. It should also be noted that the AMAD obtained with the Marple impactor was much larger than that obtained with the Sierra impactor (see Table 2). However, these data should be approached with caution as they were obtained on two different days.

We can offer no satisfactory explanation for the different performance obtained with:

a) the same type of cascade impactor sampling at the same location, but at different sampling flow-rates and with different number of impactor stages; and

b) different types of cascade impactors, i.e., Sierra and Marple impactors, sampling side by side.

It is not clear whether the differences observed in AMAD, MMAD and size distribution can be ascribed to differences in dust deposition patterns arising from different operating conditions, or to differences in the geometry of the cascade impactors used.

Figures 18 to 29 show the cumulative dust mass percentage and/or α-particle cumulative activity percentage, of size less than $D_{p,50}$, versus $D_{p,50}$ for several cascade impactors. Four physico-chemical operations were monitored, i.e., acid leaching, counter-current decantation, solvent extraction and yellowcake precipitation and drying.

Although the meaning of MMAD and AMAD has been explained above, the labels MMAD and AMAD, that appear in the graphs, are also used here to identify, respectively, dust size distribution and radioactivity size

distribution curves. The graphs drawn through direct experimental data points represent straight lines calculated by linear regression analysis. Two radioactivity size distribution graphs are sometimes shown for the Sierra impactors. In one (AMAD), data from the last three cascade stages have been ignored. The other graph, labelled $\overline{\text{AMAD}}$, has been obtained taking into account all impactor stages. The difference between both graphs at the AMAD point (i.e., 50% cumulative ordinate) is ~10%. In most cases, however, AMAD and $\overline{\text{AMAD}}$ roughly coincide, and hence only one graph is shown.

Except for data obtained with the Marple impactors, upper graphs refer to long-lived radioactive dust, whereas lower graphs refer to radon progeny (RnD), e.g., Figure 18.

Figures 18 and 19 show data for two acid leaching operations carried out on different days. Data were obtained with the same Sierra cascade impactor at the same location. The graphs show the cumulative dust mass percentage and α-particle cumulative activity percentage versus $D_{p,50}$. Data were as follows: MMAD = 6.9 (7.4) μm, AMAD (LLRD) = 6.5 (8.5) μm, $\overline{\text{AMAD}}$ (LLRD) = 6.6 (9.5) μm, and AMAD (RnD) = 0.24 (0.17) μm. The data in round brackets correspond to the second day. The data show that the AMAD for LLRD and RnD for the two days differed by about 40%. However, the only difference between the two tests was the length of the sampling period, i.e., first test lasted about 12 hours and was carried out during the day shift (7:47 to 19:37), whereas the second test lasted about 22 hours (from June 7 at 9:50 to June 8 at 7:20), and hence, was carried out through the day and night shifts.

The above difference could be partly explained by noticing that when a cascade impactor has been operating for several hours, the radon progeny that is counted at the end of the sampling period is representative, approximatively, of that collected about one mean-life before the end of the sampling period (~4 min for RaA, ~40 min for RaB, ~30 min RaC), whereas long-

lived dust activity measurements are not affected by radioactive decay. This makes it difficult to compare the AMAD and MMAD of LLRD and radon progeny, because what is counted has not necessarily been collected by the cascade impactor during the same period of time.

Figure 20 shows data for the counter-current decantation (CCD) operations at two different locations in the CCD plant. Data were obtained with two different Marple cascade impactors. The AMAD (LLRD) obtained were 12.8 μm and 10.5 μm, with an average of ~11.6 μm. The difference between these two experiments are considered to be within experimental error. Also shown in Figure 20 is the corresponding AMAD for the radon progeny, RnD. The values obtained were 0.15 μm and 0.33 μm, corresponding, respectively, to an AMAD (LLRD) of 12.8 μm and 10.5 μm, as indicated above. The large difference between those two values for the AMAD (RnD) is not surprising because of the relatively low short-lived α-particle activity counted, in the presence of relatively large backgrounds and LLRD corrections, and the short counting times that were necessary to measure the activity on the substrates before substantial radioactive decay took place.

Figure 21 shows similar data to Figure 20 (i.e., Marple impactor), but for a different location in the CCD plant. Data for the AMAD were as follows: AMAD (LLRD) = 13.1 μm and AMAD (RnD) = 0.11 μm. The average value for the AMADs calculated from Figures 20 and 21, and Table 3 are as follows: $AMAD(LLRD)_{av} = 12.1 \pm 1.4$ μm and $AMAD(RnD)_{av} = 0.2 \pm 0.1$ μm.

The data from Figures 20 , 21, and 29, obtained with the Marple impactors, show an unusual curve-shaped size distribution for the LLRD which is not shown for the case of the radon progeny. The shape of the LLRD distributions obtained with these impactors cannot be explained satisfactorily at present.

Figure 22 shows more data for the CCD operation obtained this time with

a Sierra cascade impactor. Examination of Figures 20 to 22 show that the data obtained with the two types of cascade impactors (Sierra and Marple) for CCD operations is quite consistent. An overall average for this operation taking into account all data from the Sierra and Marple impactors gives AMAD (LLRD) = 11.6 $\pm$ 1.5 μm, AMAD (RnD) = 0.20 $\pm$ 0.10 μm.

Figures 23 and 24 show data for solvent extraction operations obtained the same day with a Sierra cascade impactor (Figure 23), and a Marple cascade impactor (Figure 24). These Figures show that AMAD (LLRD) did not differ significantly for these two impactors, i.e., 4.5 μm and 3.8 μm, respectively, with an average of 4.15 μm. The AMAD (RnD), however, differed substantially, i.e., 0.4 μm and 0.58 μm (>40% difference) with an average of 0.49 μm. Notice that data from the first impactor stages have been ignored because no, or very little, radon progeny activity was associated with particulate matter above ~2 μm.

Figures 25 to 29 show data obtained with different cascade impactors (Sierra and Marple), on different days and at different locations for yellowcake precipitation operations.

Figures 25 and 26 show data for the same Sierra impactor for two different days. Although all graphs refer to the yellowcake precipitation operation, in one case sampling was conducted during the drying phase of the operation (Figure 26), whereas in the other case sampling was carried out below the yellowcake precipitation reactor (Figure 25). This may explain the differences in AMAD (LLRD) observed. Independently from the sampler location, the above Figures show that AMAD (LLRD) was substantially higher in both cases than its corresponding MMAD. The AMAD for the radon progeny (see Figure 25) was about 0.40 μm.

Figures 27 and 28 also show as Figures 25 and 26 that the AMAD (LLRD) for the yellowcake precipitation operation was significantly higher than the

MMAD of the carrier dust. The AMAD for the radon progeny was between 0.18 μm and 0.27 μm. An examination of the data from Figures 25 to 28, and Table 3 show a wide range of values for both the AMAD and MMAD. Values obtained in March were higher than values measured in June. The ratio of the maximum value to the minimum value for the AMAD and MMAD was greater than 2. It is not clear whether these differences are related to some difference in the characteristics of the uranium ore processed in March and June. It should be noted that the lowest values obtained were below the yellowcake precipitation reactor.

Figure 29 shows AMAD data for the yellowcake precipitation obtained with a Marple cascade impactor. The graph shows the corrected, for stage collecting efficiency, and non-corrected size distributions. As indicated above, the shape of the distribution is not clearly understood.

Identification of the radionuclides in the radioactive dust was done by means of α-spectrometry and γ-spectrometry.

Alpha-spectrometry on at least one sample of each mechanical and physico-chemical operation was carried out under vacuum conditions in order to improve the energy resolution of the spectra. Except for yellowcake samples, counting times in excess of 24 hours were necessary for good counting statistics.

Because of (a) self-absorption effects, i.e., α-particle absorption in dust, leading to spectrum broadening and photopeak overlapping; (b) relatively low signal-to-noise ratio; and (c) spectrometer drift, positive identification of the radionuclides in dust samples by α-spectrometry was not straightforward. A ^{241}Am source and a $^{226}Ra/^{232}Th$ source were used before and after each radioactive measurement of each dust sample. The above radioactive sources provided the following α-energy lines for α-particle identification and α-spectrometer calibration purposes:

^{241}Am : $\bar{E}_\alpha$ = 5.45 MeV

^{218}Po : $\bar{E}_\alpha$ = 6.0 MeV

^{214}Po : $\bar{E}_\alpha$ = 7.69 MeV

^{212}Po : $\bar{E}_\alpha$ = 8.78 MeV

Analysis of the data from mechanical operations samples showed three main photopeaks with the following α-particle average energies: 4.13 $\pm$ 0.22 MeV, 4.75 $\pm$ 0.32 MeV, and 7.17 $\pm$ 0.3 MeV, which can tentatively be ascribed to ^{238}U (4.3 MeV), ^{226}Ra (4.8 MeV) and ^{214}Po (7.69 MeV), see Table 5.

Identification of the high energy α-particle peak was difficult because of spectral broadening and poor statistics of counting. The contribution from ^{222}Rn (5.48 MeV) and ^{218}Po (6.00 MeV) in the samples to the α-spectrum could not be ascertained because of photopeak broadening and overlapping.

Alpha-spectra analyses from physico-chemical operations and yellowcake packaging showed two main photopeaks with the following energies: 3.99 $\pm$ 0.13 MeV and 4.46 $\pm$ 0.18 MeV. These two photopeaks can tentatively be ascribed to ^{238}U (4.2 MeV) and $^{234}U/^{230}Th$ (4.7 MeV), see Table 5. The lower α-particle energy measured for these radioisotopes is attributed to energy degradation in dust, i.e., self-absorption. Only these two peaks appear in the spectra corresponding to yellowcake precipitation, solvent extraction and yellowcake packaging. Counter-current decantation and acid leaching spectra also show a much smaller photopeak of higher energy which could not be unambiguously identified.

The radioisotope identification indicated above assumes little or no thorium present in the dust samples. This assumption is supported by open-face radon progeny grab-sampling measurements 40 min and 7 h after sampling. These measurements showed negligible residual α-activity after the radon progeny decayed away.

Figure 2 shows α-particle spectra corresponding to three different mill operations, namely: cone crushing, yellowcake precipitation and yellowcake packaging. The difference in photopeak α-energy location is ascribed, as indicated above, to self-absorption.

Dust samples from all the mill mechanical operations were analyzed by γ-spectrometry. However, despite the very high resolution of the apparatus (0.5 keV/channel), positive identification of the radionuclides in the dust samples was rather difficult even after counting for extended periods. The reason for this is the low radioactivity in the samples and the relatively large natural background. (The activity of the samples is related to the sampling time which determines the amount of dust collected at a given flow-rate, and the ore grade.) Although many peaks were found in the samples, only the radioisotopes ^{214}Pb and ^{210}Pb could be identified with reasonable certainty as belonging to the samples and not to background. Table 6 shows γ-ray energies corresponding to some radioisotopes of interest of the natural uranium radioactive chain.

Because of the relatively large amount of dust generated in yellowcake packaging, the activity of the samples from this operation was easily measurable and the radioisotope make-up could be quite confidently identified. The following radioisotopes were identified: ^{234}Th, ^{234m}Pa, ^{234}U, ^{230}Th and some ^{226}Ra, ^{210}Pb and ^{235}U. The radioisotope composition for physico-chemical operations was somewhat similar but the activity considerably smaller, a fact that made identification somewhat difficult at times (see Table 6).

Table 7 shows total and respirable dust measurements for several mechanical operations. Measurements were conducted using open-face filter and nylon cyclone samplers. The values for total dust are in fair agreement with data using the cascade impactors (see Table 2). Respirable dust concentrations were, of course, substantially lower than total dust

concentration.

Figure 30 shows the respirable dust concentration (mg/m^3) measured during several physico-chemical operations with a real-time, passive, continuous dust monitor model Mini-Ram PDM-3 manufactured by GCA U.S.A.). Three operations were monitored: counter-current decantation, acid leaching and yellowcake precipitation. The dust concentration was highly variable but was in general below 1 mg/m^3. The lowest dust concentration was found in yellowcake precipitation. Apart from the three operations indicated above, no other physico-chemical operations were monitored with the Mini-Ram.

Radon progeny data for several mechanical operations are shown in Tables 8 and 9. Radon progeny Working Level data ranged from a few mWL up to about 67 mWL. The relatively low values for the ratios [^{214}Pb]/[^{218}Po] and [^{214}Bi]/[^{218}Po], in most cases, indicate the presence of reasonably 'young air', as expected in a well ventilated area. Table 8 shows data obtained with a continuous Working Level monitor WLM-300 manufactured by EDA Instruments (Toronto). Table 9 shows grab-sampling data obtained by the Thomas-Tsivoglou method. The data for the yellowcake packaging operation have been calculated assuming the α-count recorded as totally originating from ^{218}Po and ^{214}Po. It should be noted that this is not true as a large fraction of the α-activity arises from LLRD. This fact is reflected in the unusual data presented.

Figure 31 shows radon progeny Working Level measurements conducted with the WLM-300 monitor for several physico-chemical operations. In general, the Working Level (WL) measured was low, and as for the case of mechanical operations, it rarely exceeded 50-60 mWL, and for short periods of time. The highest measured WL was during yellowcake precipitation and acid leaching operations. Lower radiation levels were measured at other locations and operations. The lowest WL measurements were in counter-current decantation and in solvent extraction operations.

The data of Tables 8 and 9, and Figure 31 are not directly comparable as they were taken at two different periods, i.e., March and June, respectively, for which the air dilution factors or ventilation and climatological conditions were substantially different.

SUMMARY AND CONCLUSIONS

From this study the following conclusions can be drawn. The AMAD corresponding to the long-lived radioactive dust was, in general, slightly larger than the corresponding MMAD of the carrier dust.

The MMAD and AMAD calculated for the dust cloud depended on the type of mechanical and physico-chemical operations in the mill. The values for these two diameters were in the range 3 to 19 μm.

The AMAD corresponding to the radon progeny was in the submicron range, i.e., 0.11 to 0.7 μm. It should be indicated that the AMAD corresponding to the radon progeny is best measured using diffusion batteries. Hence, the data presented here obtained with cascade impactors are assumed to be accurate (at best) to a first approximation only. The reason for using cascade impactors is simply that they were available for LLRD measurements.

Differences were found for the MMAD and AMAD obtained at the same location with different types of cascade impactors, or using the same kind of impactors but sampling under different operating conditions. It is suggested that this topic should be further investigated.

The long-lived radioactive dust concentration depended on the mechanical operation. It was highest for the grizzly (TP1), and yellowcake packaging (TP7) operation, followed by some crushing operations, e.g., jaw-crusher (TP2).

Alpha-particle self-absorption, i.e., absorption in dust, was a problem for some samples when the mass collected in some impactor stages, in certain

mechanical operations, was higher than a critical value. Hence, errors should be minimized by choosing sampling times consistent with adequate dust mass collection for accurate calculation of the MMAD, and low α-particle self-absorption for precise determination of the AMAD. Alternatively, use could be made of liquid scintillation counting and/or neutron activation analysis.

Identification of radionuclides by α-spectrometry and γ-spectrometry was not straightforward, except for yellowcake packaging, because of the low specific activity of some of the samples. Some of the following radionuclides were tentatively identified depending on the sample, i.e., mill operation: ^{238}U, ^{226}Ra, ^{234}U, ^{230}Th, ^{235}U, ^{234m}Pa, ^{234}Th, ^{214}Po, ^{214}Pb and ^{210}Pb.

Knowledge of the AMAD and LLRD radionuclide composition permits the estimation of some important health risk indices and radiation exposure variables such as the annual limit of intake (ALI).

ACKNOWLEDGEMENTS

This study was requested and partly supported by Atomic Energy Control Board (AECB). The authors would like to acknowledge the technical assistance of E. Edwardson in conducting experimental work and assisting in some calculations. The authors would also like to thank Mr. T. Meadley (AMOK Ltd., Saskatoon) for his cooperation throughout this study. Finally, the authors would like to acknowledge the assistance of some of the staff at Cluff Lake Mining during this field investigation.

REFERENCES

1. Bigu, J. and Grenier, M.G., "Studies of radioactive dust in Canadian uranium mines"; CIM Bull, vol. 77, pp 62-68; 1984.

2. Duport, P.J. and Edwardson, E., "Characterization of radioactive long-lived dust present in uranium mine and mill atmospheres"; in Proc Occup

Radiation Safety in Mining, vol. 1, pp 189-195; Canadian Nuclear Association (Toronto), H. Stocker (Ed.); 1985.

3. Bigu, J. and Grenier, M.G., "Characterization of radioactive dust in Canadian underground uranium mines"; Proc 2nd Ventilation Congr, Reno, Nevada, pp 269-277; A.A. Balkema, Rotterdam, P. Mousset-Jones (Ed.); 1985.

4. Hinds, W.C., Liu, W.V. and Froines, J.R., "Particle bounce in a personal cascade impactor"; Am Ind Hyg Assoc J, vol 46, No. 9, pp 517-523; 1985.

5. Barzic, J.Y., "Etude de l'aerosol d'une mine d'uranium"; Ph.D. Thesis, L'Universite de Bretagne Occidentale (France), 1975.

Table 1 - Cascade impactors operating characteristics

Impactor	Sampling Flow-Rate L/min	Stage Number	Cut-Off Size μm
EMR*	3.3	1	26
		2	16
		3	6.4
		4	3.8
		5	2.5
		6	1.4
		7	0.8
		8	0.5
		9	0.3
		10	0.06
C	10.5	1	14.8
		2	8.8
		3	3.5
		4	2.1
		5	1.4
		6	0.8
		7	0.4
		8	0.23
M_1 & M_2	2.0	1	21.3
		2	14.8
		3	9.8
		4	6.0
		5	3.5
		6	1.55
		7	0.93
		8	0.52

*In June, the EMR impactor was operated at a sampling flow rate of 10.5 L/min. The cut-off sizes for this case are the same as those corresponding to C.

Table 2 - Cascade impactors data for several mechanical operations in a uranium mill.

Mechanical Operation	Date 1985	Impactor	MMAD µm	Dust σg	AMAD(LLRD) µm	LLRD σg	AMAD(RnD) µm	RnD σg	Dust Conc. mg/m^3	LLRD Conc. mBq/m^3	LLRD(S.A.) mBq/mg
Grizzly (TP1)	March 22	C	15.4	2.8	15.3	3.4	0.66	9.1	12.51	1090	87
" "	"	EMR	14.5	2.4	19.0	3.0	0.69	2.6	8.99	1570	175
Jaw Crusher (TP2)	March 23	C	12.8	3.0	12.3	3.3	0.26	6.5	2.70	380	141
" " "	"	EMR	8.4	2.7	7.6	3.7	0.16	13.6	1.53	380	248
Cone Crusher (TP4)	March 25	C	5.4	2.6	5.7	2.8	-	-	0.84	190	226
" " "	"	EMR	6.6	2.4	6.2	3.4	-	-	0.86	270	314
Screens (TP3)	March 24	C	5.3	2.3	5.8	2.6	0.58	4.7	1.69	390	231
" "	"	EMR	6.2	2.4	5.7	3.0	0.69	4.6	1.49	520	349
Top Fine Ore Bin/	March 26	C	4.0	3.3	4.0	3.3	0.31	7.1	0.30	180	600
Conveyor Belt #8 (TP5)	"	EMR	3.7	4.5	4.1	3.5	0.14	13.6	0.37	230	605
" "	June 8	EMR	3.4	2.8	3.8	3.1	-	-	0.08	100	1250
Grinding (TP6)	June 5	EMR	-	-	3.7	5.8	0.20	10.5	-	48	-
" "	June 7	M_2	-	-	10.0	2.3	-	-	-	59	-
Yellowcake Packaging	March 22	C	10.5	3.1	11.1	3.5	-	-	12.43	1.3×10^5	1.05×10^4
(TP7)	"	EMR	12.3	3.7	11.8	2.6	-	-	6.21	1.25×10^5	2.01×10^4

Notes: a) C and EMR are Sierra impactors. M_2 is a Marple impactor.
b) σg represents geometric standard deviation (µm).
c) RnD stands for radon progeny.
d) S.A. indicates specific activity.

Table 3 - Cascade impactors data for several physico-chemical operations in a uranium mill.

Operation	Date	Impactor	MMAD (μm)	Dust σg	AMAD(LLRD) (μm)	LLRD σg	AMAD(RnD) (μm)	RnD σg	Dust Conc. mg/m^3	LLRD Conc. mBq/m^3	LLRD(S.A.) mBq/mg
Acid Leaching	June 5	C	6.9	2.4	6.6	3.5	0.24	4.0	0.30	252	840
" "	June 7	C	7.4	2.8	9.5	4.0	0.17	4.2	0.23	181	787
Counter-Current Decantation (CCD)	June 7	EMR	8.3	3.0	10.2	3.6	0.21	3.0	0.40	266	665
	June 5	M_1	-	-	12.8	1.7	0.15	33.0	-	394	-
"	June 5	M_2	-	-	10.5	1.8	0.33	16.0	-	371	-
"	June 6	M_1	-	-	13.1	1.8	0.11	14.7	-	160	-
Solvent Extraction	June 6	EMR	4.5	5.3	2.9	3.7	0.40	3.3	0.06	39	650
" "	June 6	M_2	-	-	3.8	3.9	0.58	2.8	-	31	-
Yellowcake Precip.	March 27	C	7.0	4.0	16.2	3.8	0.27	5.0	0.34	2110	6206
" "	March 27	EMR	9.0	2.8	13.2	3.6	0.18	8.3	0.31	1890	6097
" "	June 8	C	5.4	6.3	9.0	4.7	-	-	0.30	134	447
" "	June 7	M_1	-	-	13.2	1.8	-	-	-	106	-
" "	June 6	C	4.0	3.8	6.6	4.9	0.40	10.8	0.06	35	583
Yellowcake Packaging	March 22	C	10.5	3.1	11.1	3.5	-	-	12.43	1.30×10^5	1.05×10^4
" "	March 22	EMR	12.3	3.7	11.8	2.6	-	-	6.21	1.25×10^5	2.01×10^4

Notes: a) C and EMR are Sierra impactors; M_1 and M_2 are Marple impactors.
b) σg represents geometric standard deviation.
c) RnD stands for radon progeny.
d) S.A. indicates specific activity.
e) Yellowcake packaging data have been included for completeness.

Table 4 - Average values of MMAD and AMAD for different mill operations.

Mill Operation	MMAD μm	AMAD μm
Grizzly	14.95	17.15
Jaw Crusher	10.60	9.95
Cone Crusher	6.00	5.95
Screens	5.75	5.75
Ore Bin/Conveyor Belt	3.70	3.97
Grinder	-	6.85
Acid leaching	7.15	8.05
CCD	8.3	11.65 ± 1.51
Solvent extraction	4.5	3.35
Yellowcake precipitation	6.35 ± 2.15	11.64 ± 3.8
Yellowcake packaging	11.4	11.45

Table 5 - Alpha-particle energy corresponding to some members of the uranium and thorium natural radioactive chains.

Radioisotope	Symbol	α-Energy MeV	Remarks
Thorium	^{232}Th	4.08	Long-lived
Thorium	^{228}Th	5.52	" "
Radium	^{224}Th	5.79	" "
Thoron	^{220}Rn	6.28	Short-lived
Thorium A	^{216}Po	6.80	" "
Thorium C	^{212}Bi	6.05	" "
Thorium C'	^{212}Po	8.78	" "
Uranium	^{238}U	4.2	Long-Lived
Uranium	^{234}U	4.7	" "
Thorium	^{230}Th	4.7	" "
Radium	^{226}Ra	4.8	" "
Radon	^{222}Rn	5.49	Short-lived
Radium A	^{218}Po	∿6.0	" "
Radium C'	^{214}Po	7.68	" "
Radium F	^{210}Po	5.30	" "

Table 6 - Gamma-energy (main peak) of some of the radioisotopes identified in dust samples from several mill operations*.

Radioisotope	Symbol	γ-Energy keV	Remarks
Lead	^{210}Pb	46.50	Long-lived (medium)
Lead	^{214}Pb	241.91	Short-lived
		295.40	" "
		351.90	" "
Bismuth	^{214}Bi	609.32	Short-lived
Thorium	^{234}Th	63.29	Long-lived
		92.38	" "
		92.80	" "
Thorium	^{230}Th	67.73	Long-lived
		143.60	" "
		185.80	" "
Uranium	^{234}U	53.00	" "
Uranium	^{235}U	84.24	Long-lived
		143.76	" "
		185.71	" "
		205.00	" "
Radium	^{226}Ra	185.99	Long-lived
Palladium	^{234m}Pa	1001.40	Long-lived

* Not all the gamma energies shown in the Table have been identified. ^{226}Ra, ^{210}Pb and ^{235}U identification is tentative.

Table 7 - Total and respirable dust concentration during some milling mechanical operations.

Location	Total Dust[1] (mg/m^3)	Respirable Dust[2] (mg/m^3)
Jaw crusher (TP2)	2.16	0.28
Screens (TP3)	1.58	0.41
Cone crusher (TP4)	0.83	0.11
Conveyor Belt/ Fine Ore Bin (TP5)	0.23	0.16

[1] Using an open-face filter holder.

[2] Using a nylon cyclone.

Table 8 - Working Level measured by a WLM-300 continuous Working Level Monitor at several locations.

Location	Date	WL* (mWL)
Grizzly (TP1)	March 22-23/85	15.3±3.3
Jaw Crusher (TP2)	March 23-24/85	16.0±1.5
Cone Crusher (TP4)	March 25-26/85	48.4±4.2
Screens (TP3)	March 24-25/85	54.7±11.1
Conveyor Belt/ Fine Ore Bin (TP5)	March 26-27/85	66.5±5.0

* Average value calculated over a 14 h period.

Table 9 - Radon progeny grab-sampling data by Thomas-Tsivoglou method at several locations.

Location	Time	WL (mWL)	$[^{218}Po]$ (pCi/L)	$[^{214}Pb]$ (pCi/L)	$[^{214}Bi]$ (pCi/L)	$[^{214}Pb]/[^{218}Po]$	$[^{214}Bi]/[^{218}Po]$	Date
Grizzly (TP1)	18:05	4.0	1.49	0.34	0.21	0.23	0.14	March 22/85
	20:44	5.8	2.96	0.19	0.48	0.06	0.16	"
	21:57	9.3	5.52	0.62	0.12	0.11	0.02	"
Jaw Crusher (TP2)	20:23	13.4	3.78	1.58	0.41	0.42	0.11	March 23/85
	20:58	13.3	1.69	1.20	1.46	0.71	0.86	"
	21:35	16.8	5.56	1.42	1.03	0.26	0.19	"
	22:10	18.4	6.73	1.79	0.64	0.27	0.10	"
Screens (TP3)	20:36	33.7	11.57	3.45	1.15	0.30	0.10	March 24/85
	21:12	36.5	14.66	4.25	-0.05	0.29	-	"
	21:47	34.7	9.92	2.73	2.85	0.28	0.29	"
	22:25	34.1	12.01	3.36	1.25	0.28	0.10	"
Yellowcake Packaging* (TP7)	19:57	19.6	0.95	2.68	1.34	2.82	1.41	March 22/85
	20:55	15.1	-1.79	1.02	3.16	-	-	"
	21:36	14.1	-0.18	0.41	3.28	-	-	"

* Data calculated assuming α-count recorded as originating from ^{218}Po and ^{214}Po.

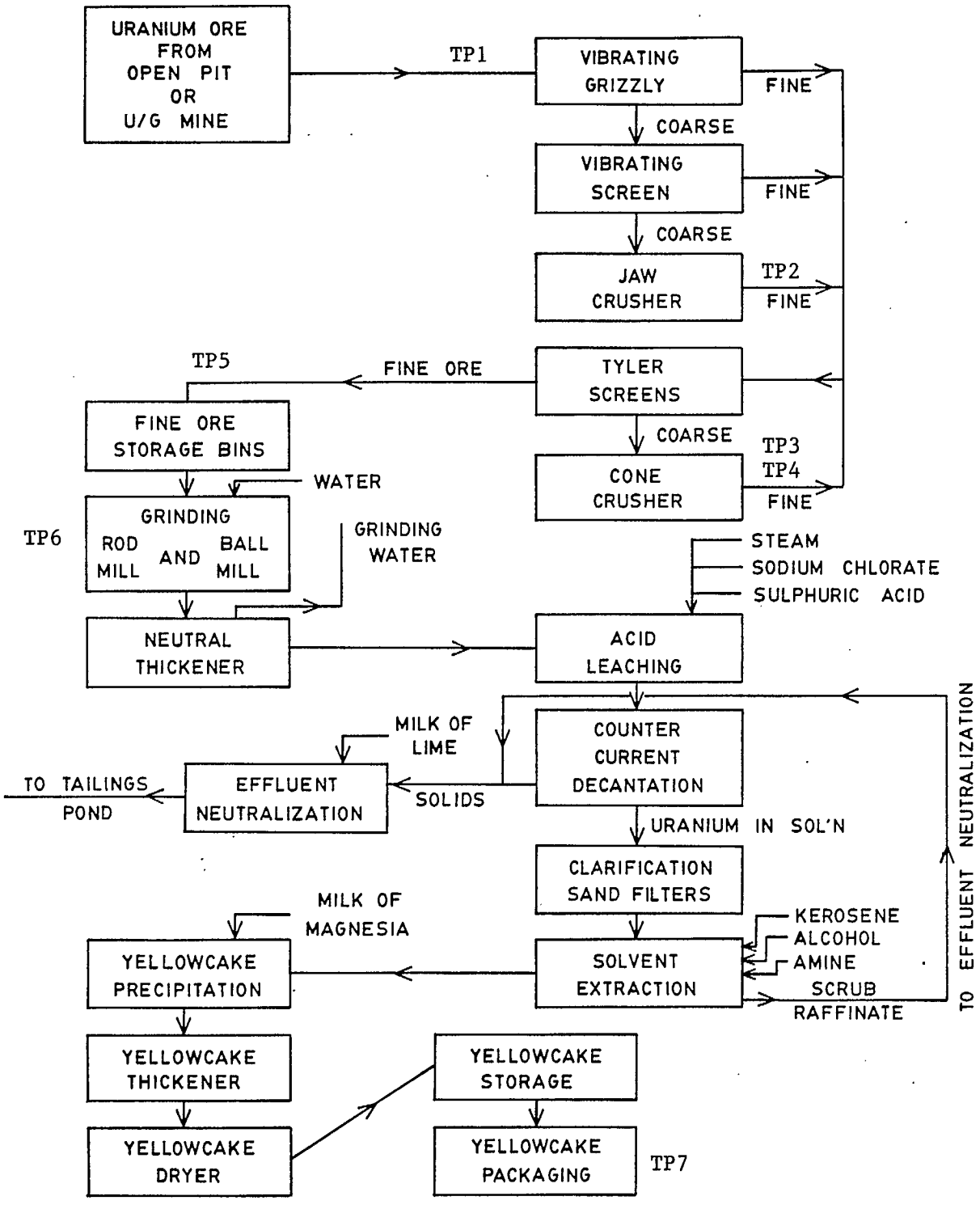

Fig. 1 - Block diagram of mechanical and physico-chemical operations in a uranium mill.

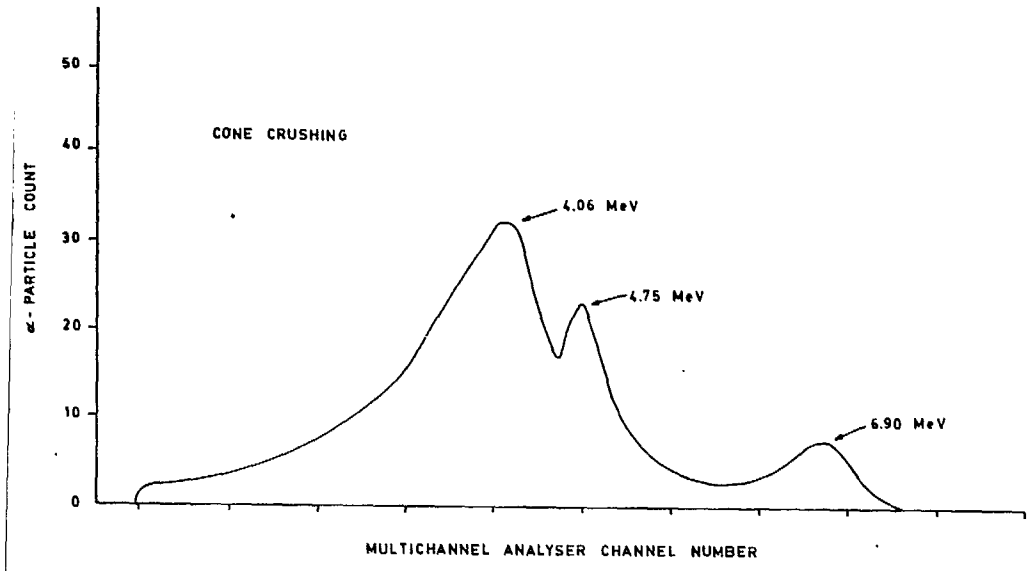

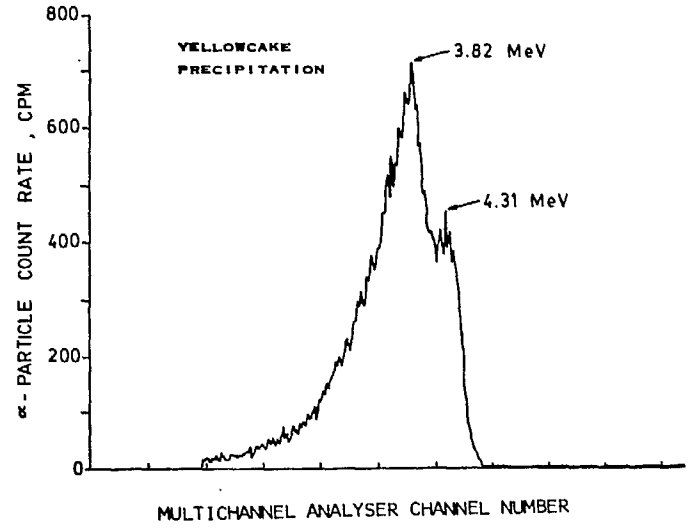

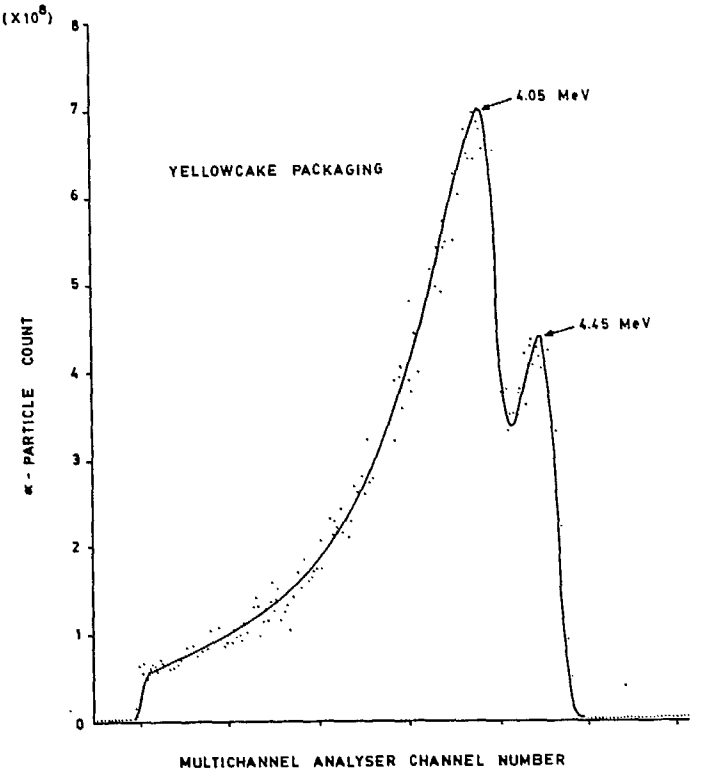

Fig 2 - Alpha-particle spectra corresponding to different mill operations.

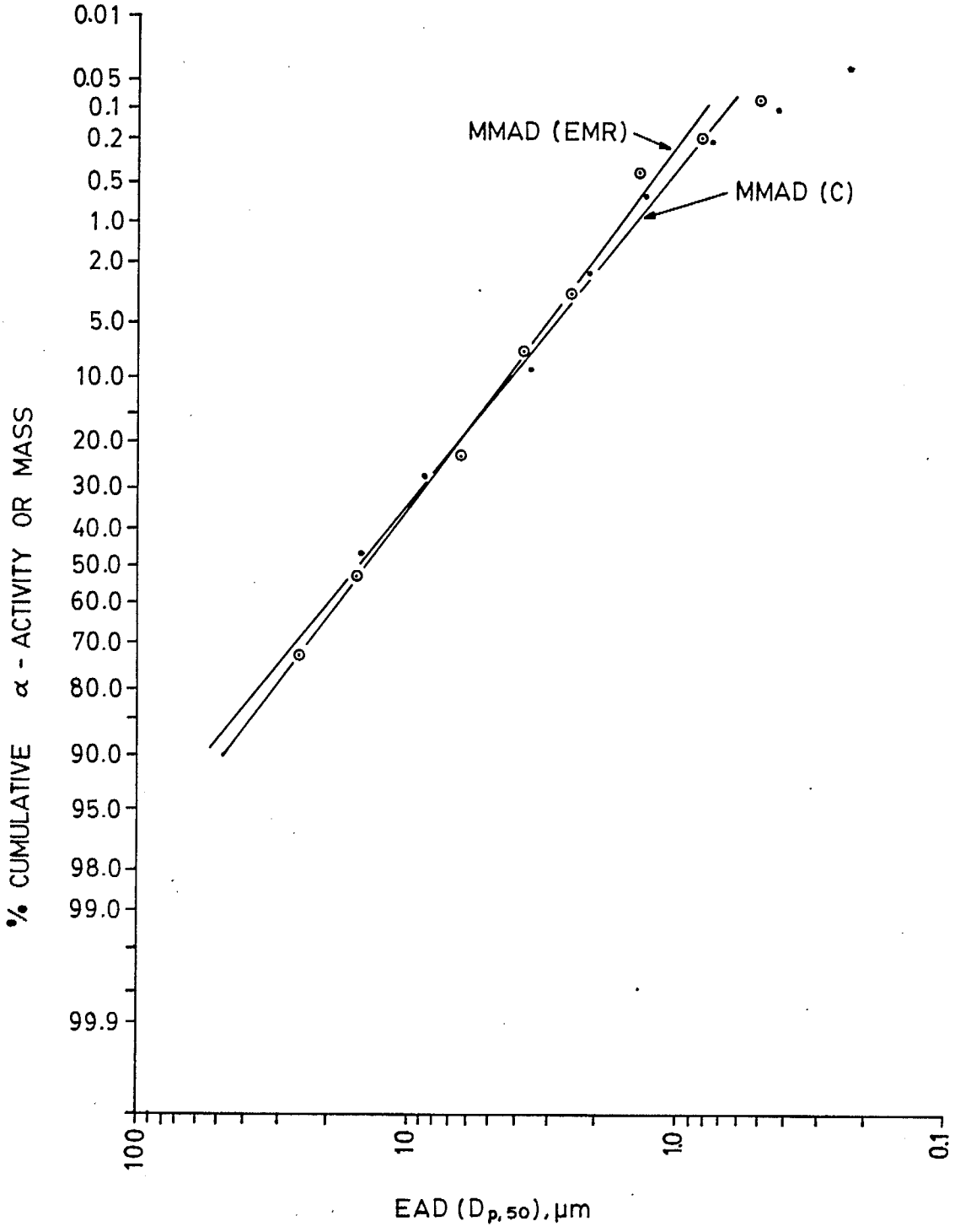

Fig. 3 - Percentage cumulative dust versus EAD for the 'grizzly' fragmentation operation.

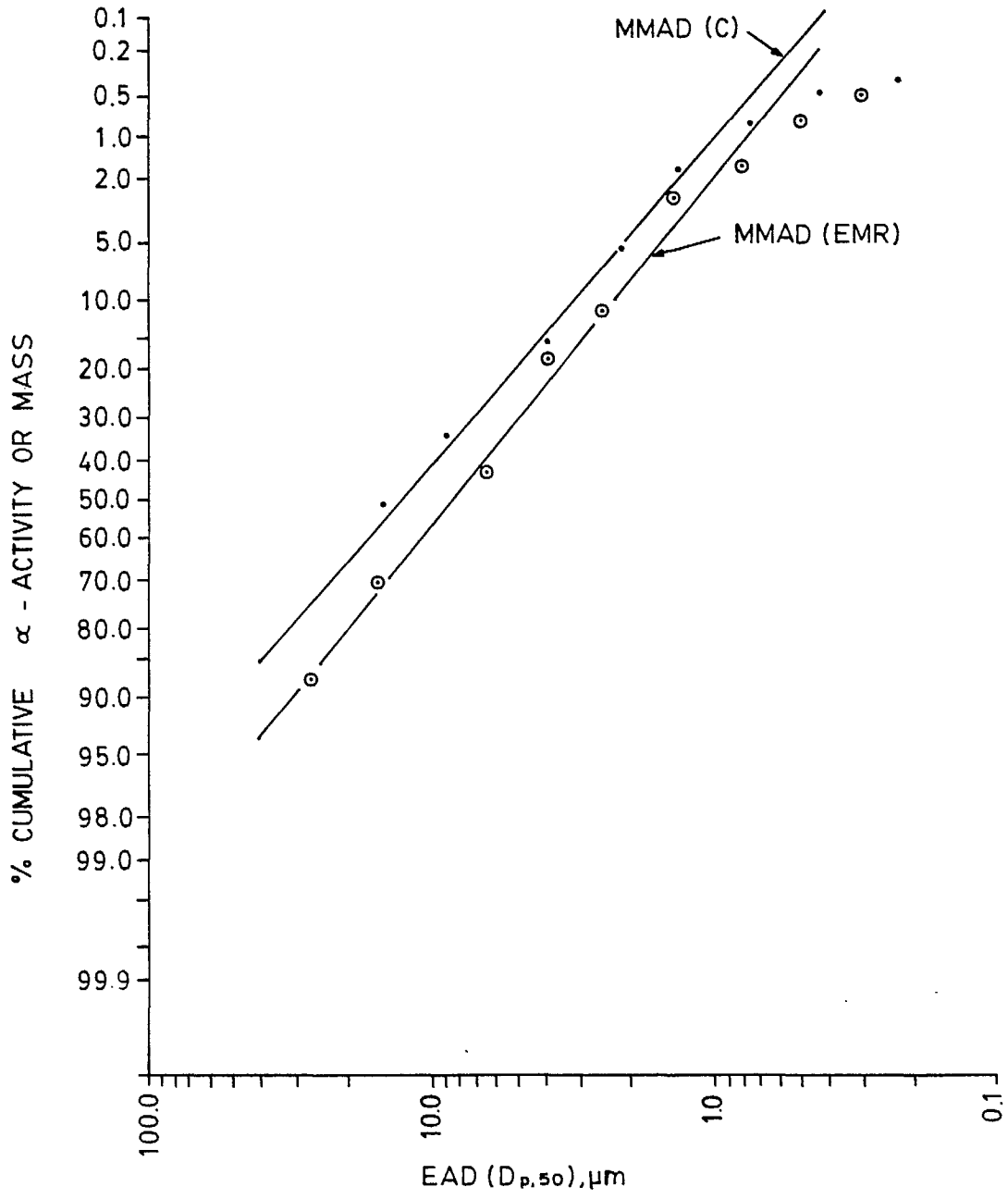

Fig. 4 - Percentage cumulative dust versus EAD for the jaw crusher operation.

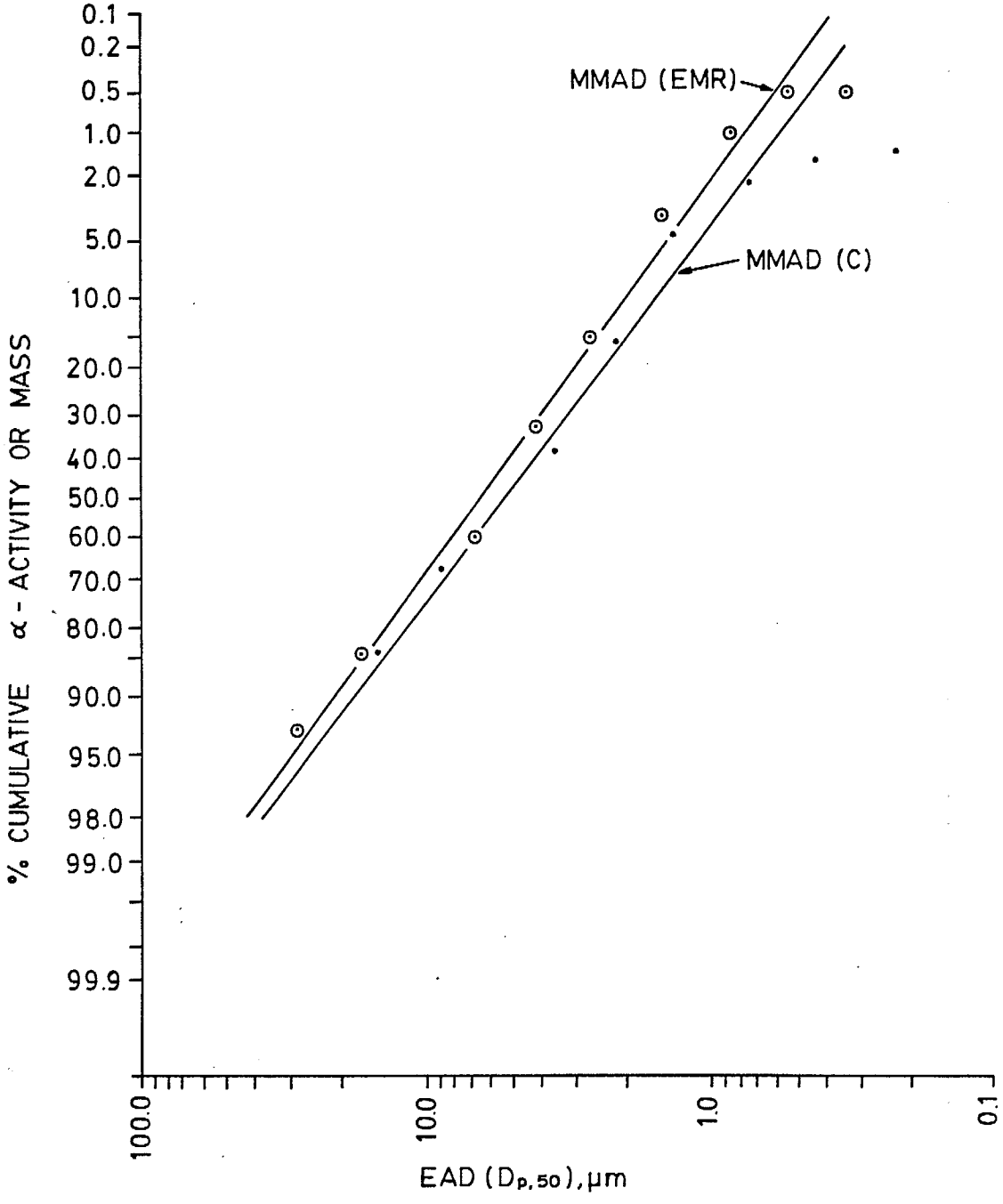

Fig. 5 - Percentage cumulative dust versus EAD for the cone crusher operation.

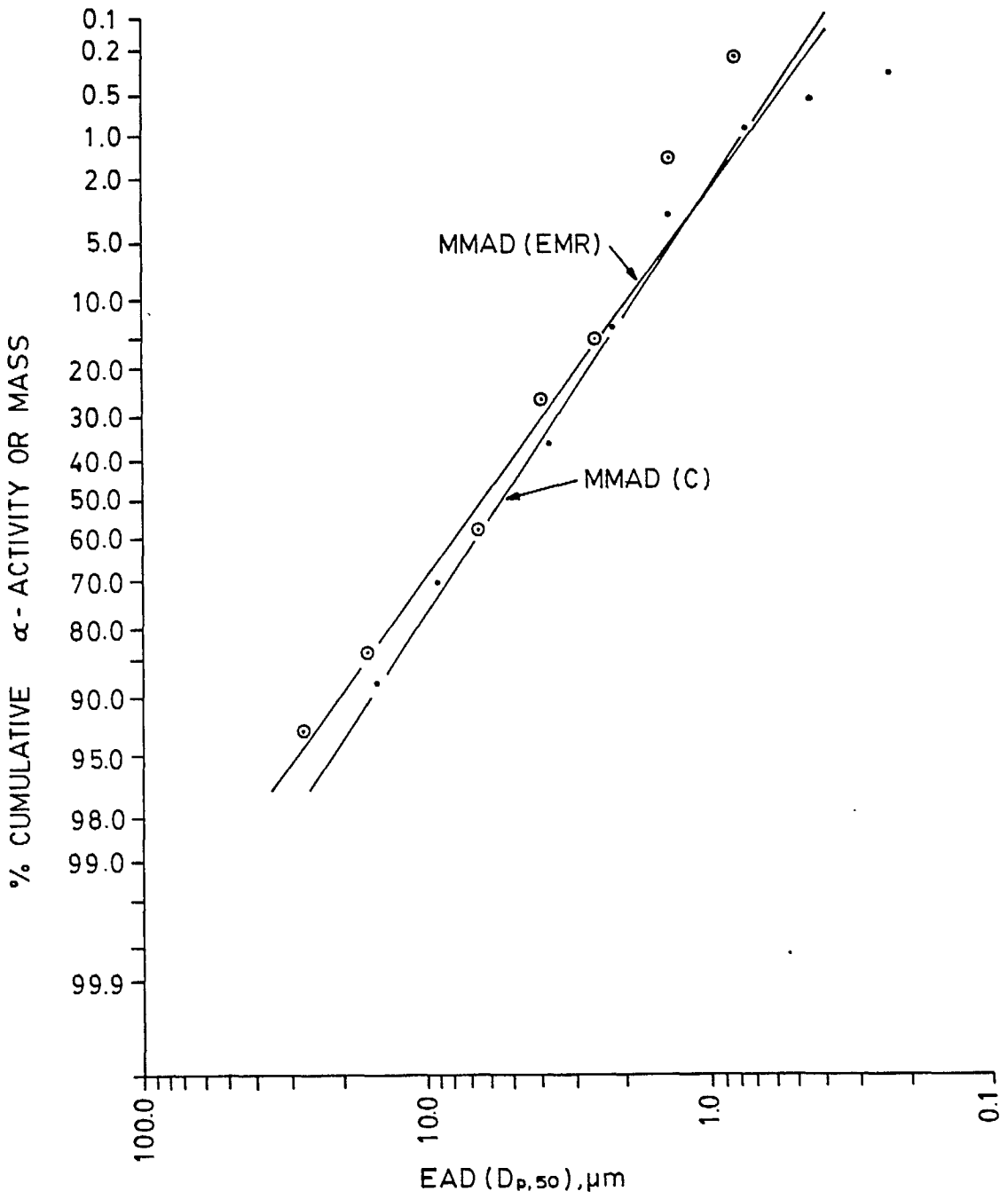

Fig. 6 - Percentage cumulative dust versus EAD for screening operations.

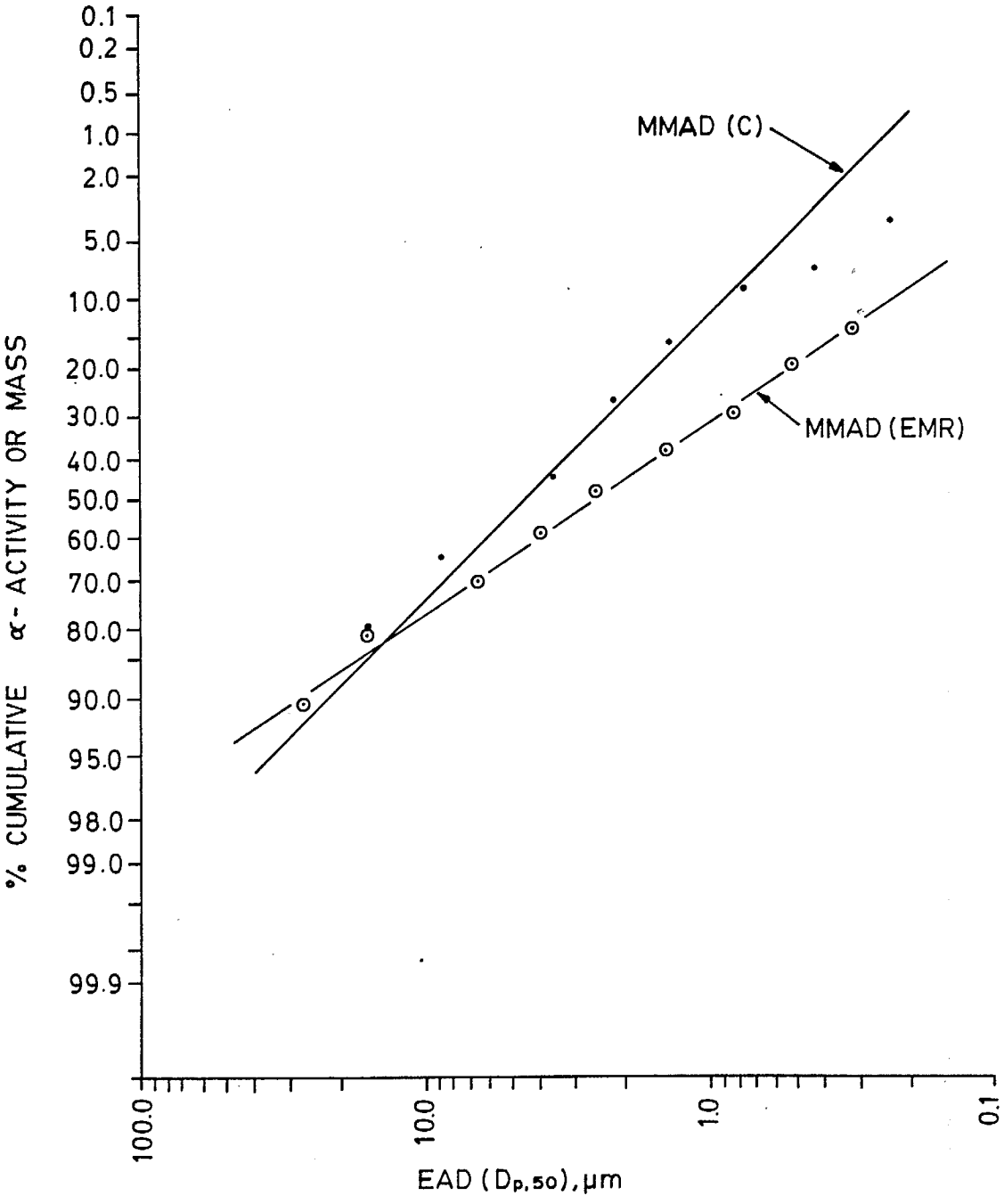

Fig. 7 - Percentage cumulative dust versus EAD for the fine ore bin/conveyor belt.

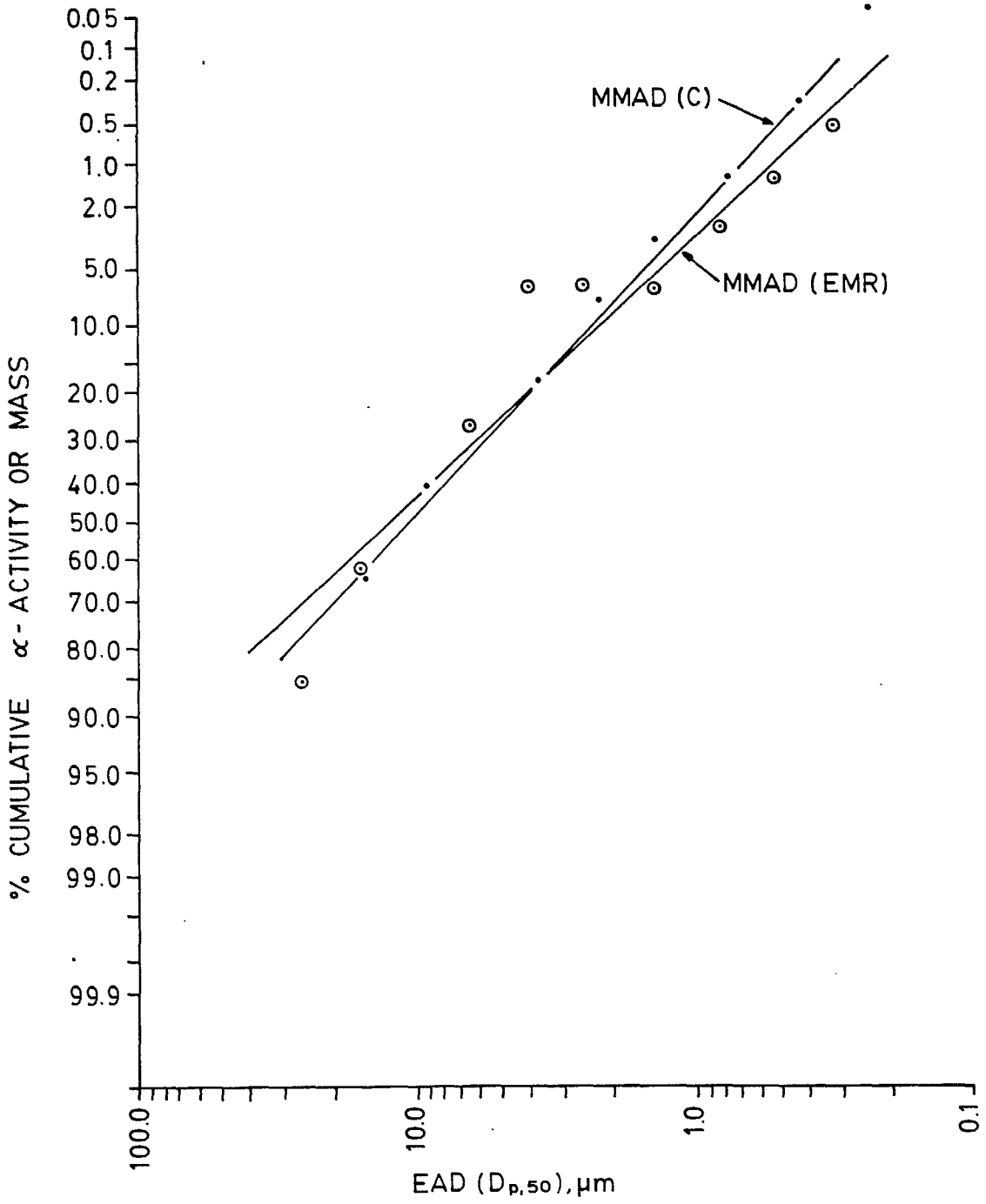

Fig. 8 - Percentage cumulative dust versus EAD for the yellowcake packaging operation.

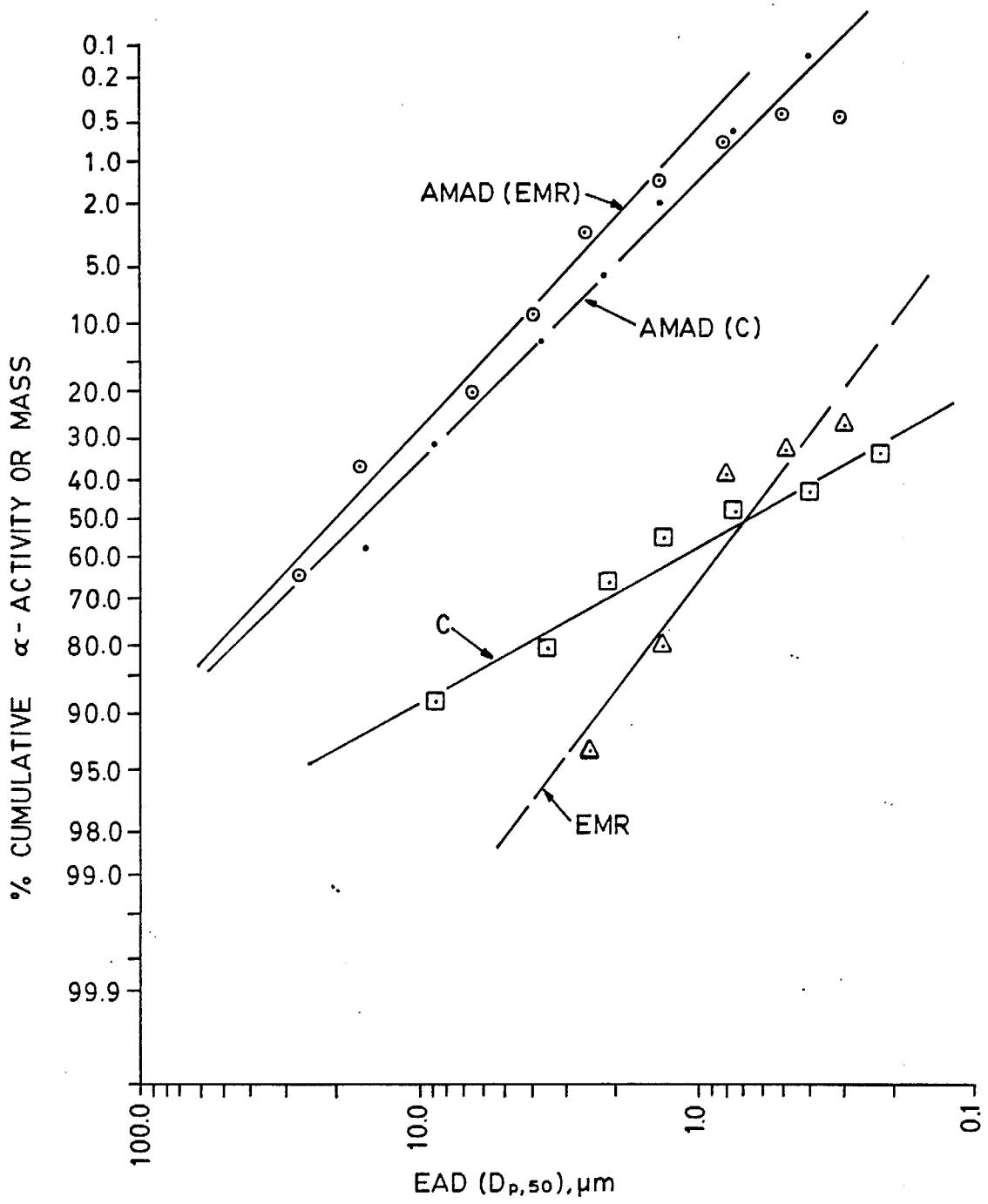

Fig. 9 - Percentage cumulative LLRD (upper graphs) and radon progeny (lower graphs) α-activity versus EAD for the 'grizzly' fragmentation operation.

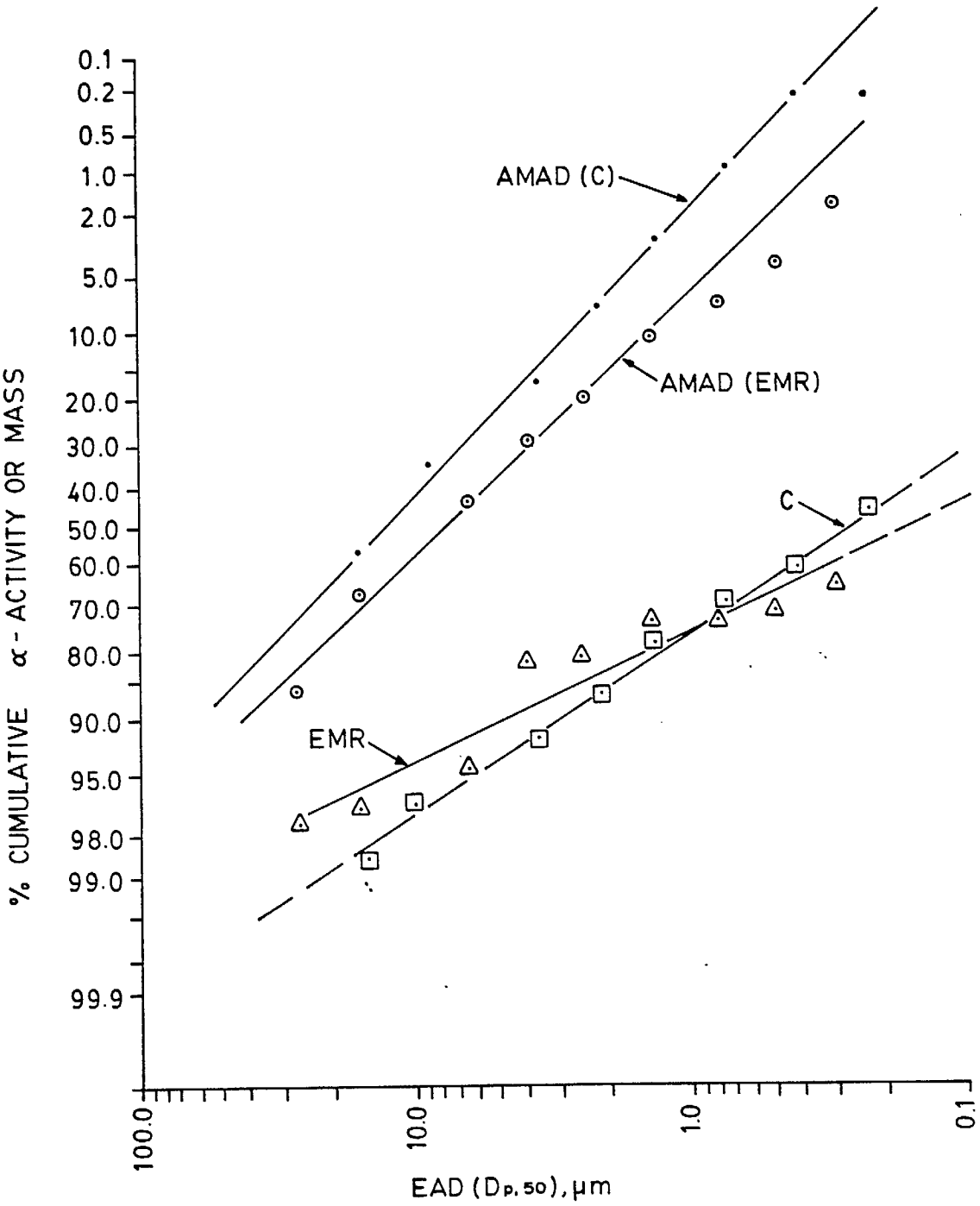

Fig. 10 - Percentage cumulative LLRD (upper graphs) and radon progeny (lower graphs) α-activity versus EAD for the jaw crusher.

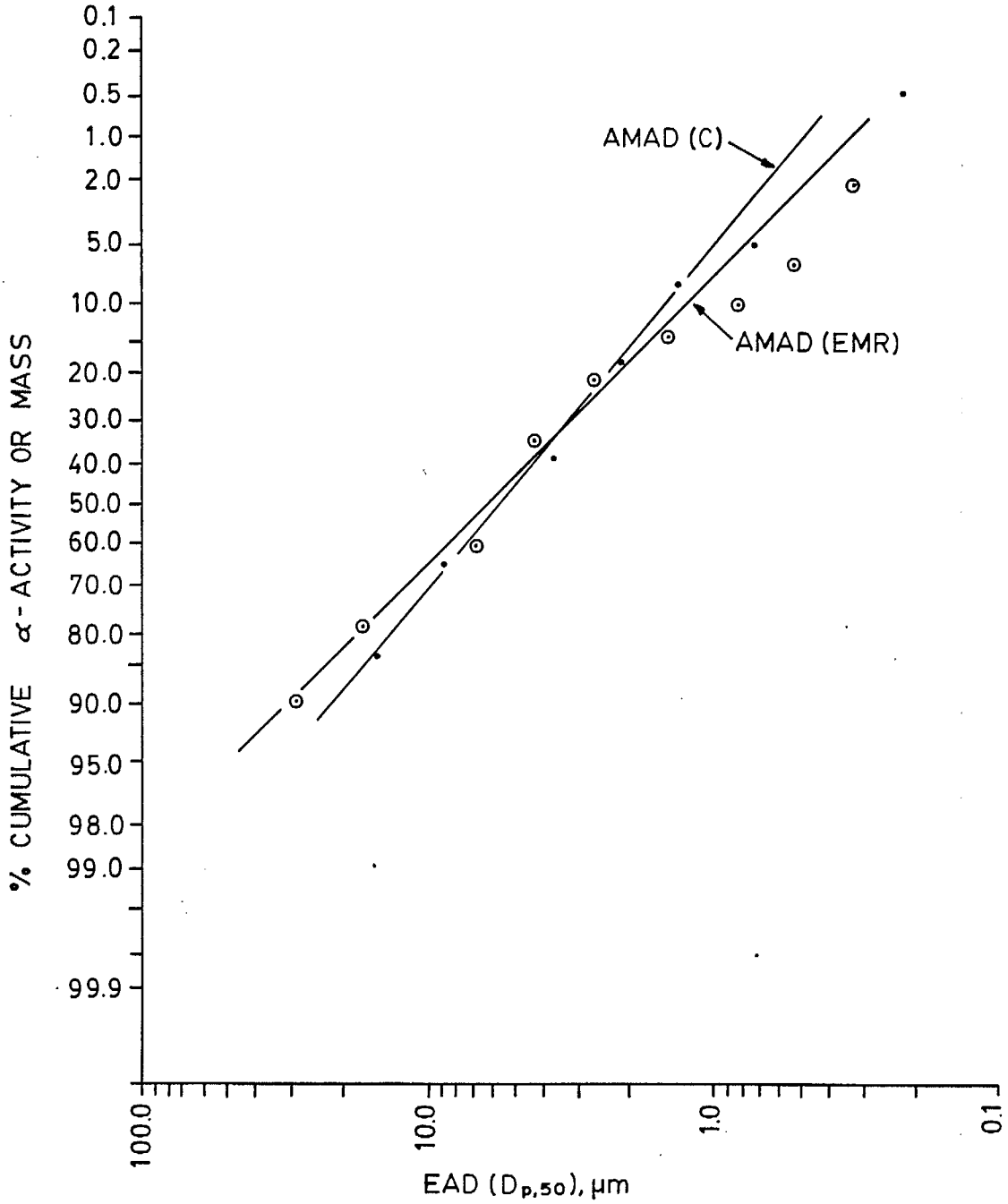

Fig. 11 - Percentage cumulative LLRD α-activity versus EAD for the cone crusher.

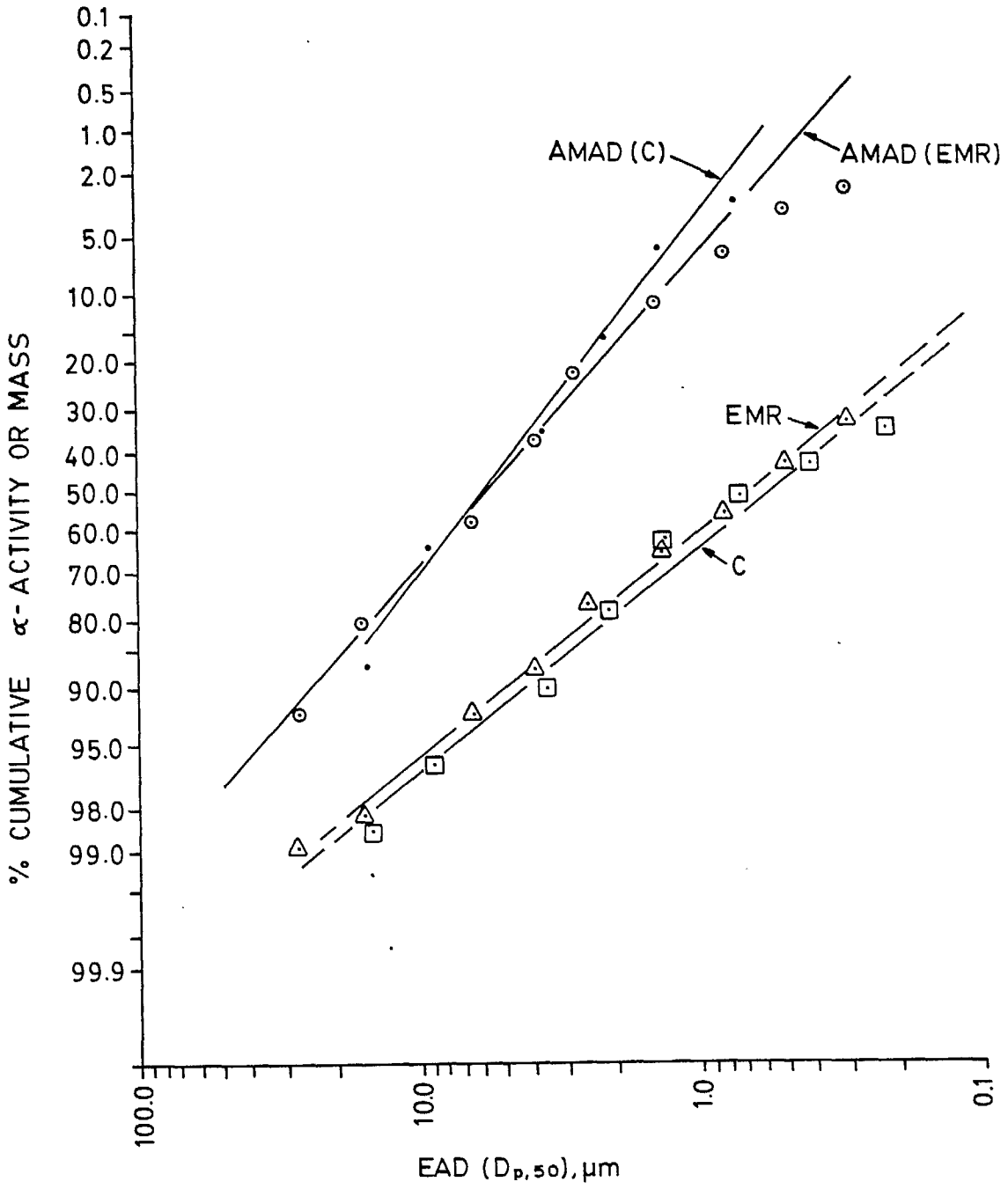

Fig. 12 - Percentage cumulative LLRD (upper graphs) and radon progeny (lower graphs) α-activity versus EAD for the screening operations.

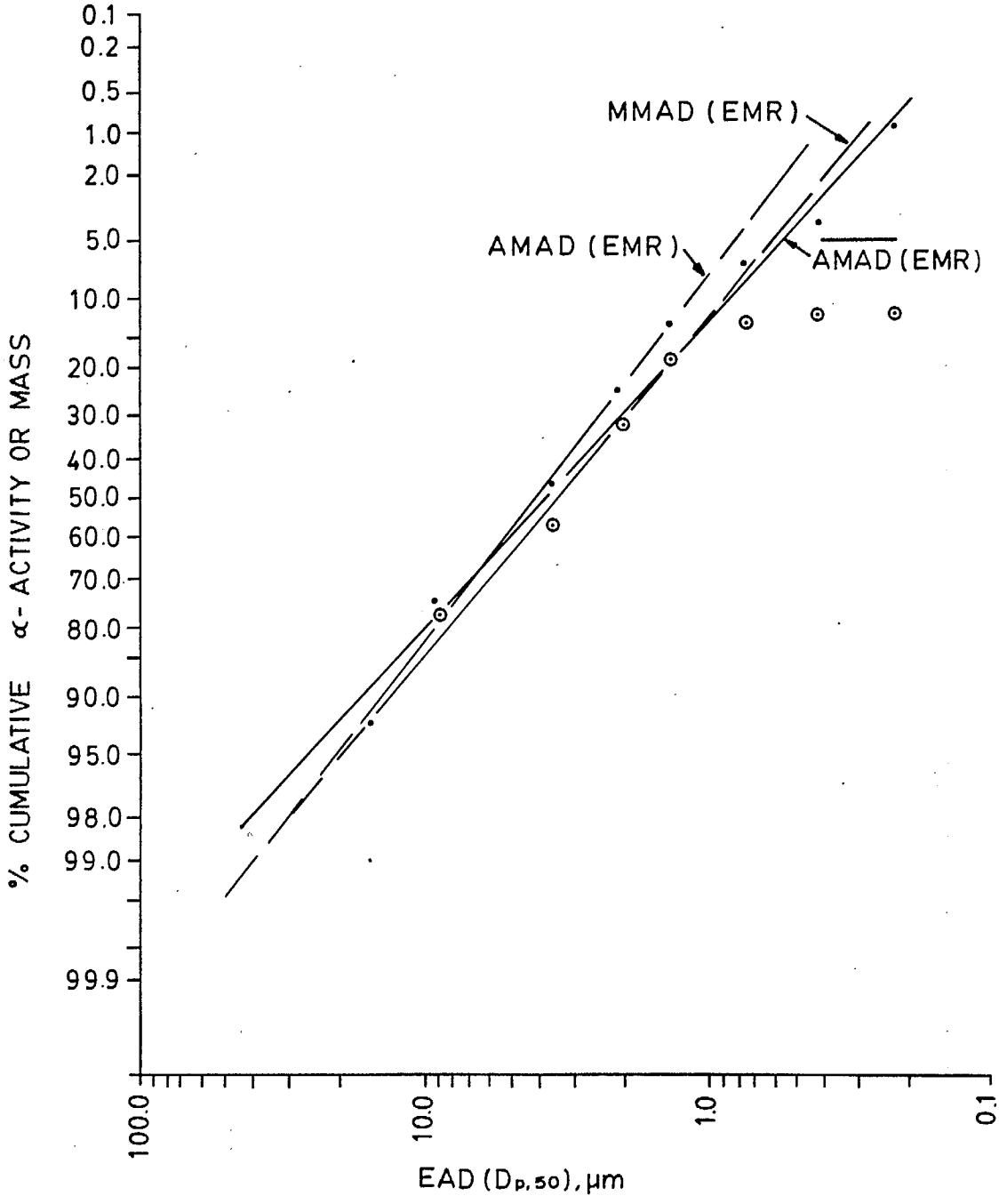

Fig. 13 - Percentage cumulative dust (MMAD) and percentage cumulative LLRD (AMAD) α-activity versus EDA for the fine ore bin/conveyor belt operation.

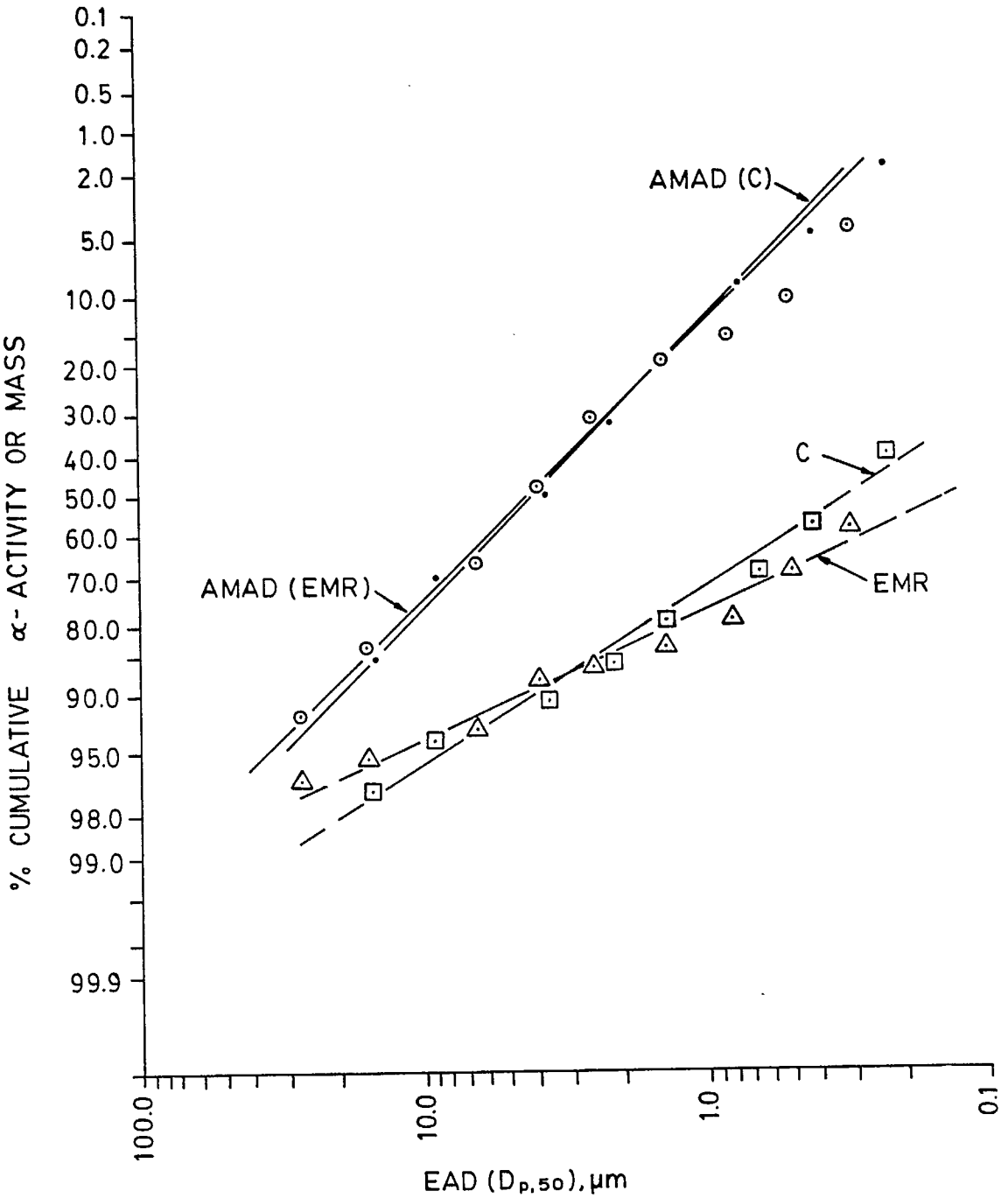

Fig. 14 - Percentage cumulative LLRD (upper graphs) and radon progeny (lower graphs) α-activity versus EAD for the fine ore bin/conveyor belt operation.

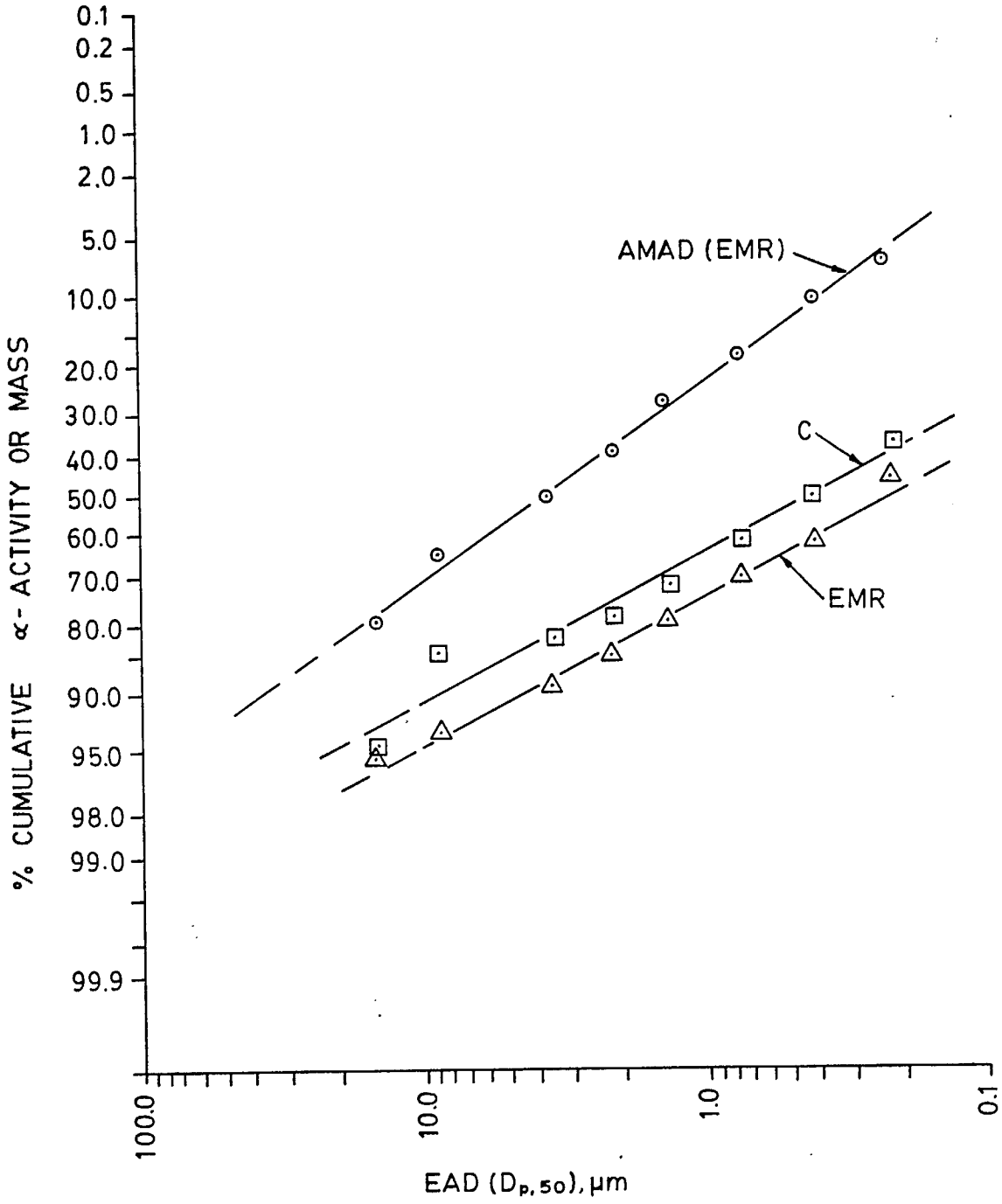

Fig. 15 - Percentage cumulative LLRD (upper graph) and radon progeny (lower graphs) α-activity versus EAD for the grinding operation.

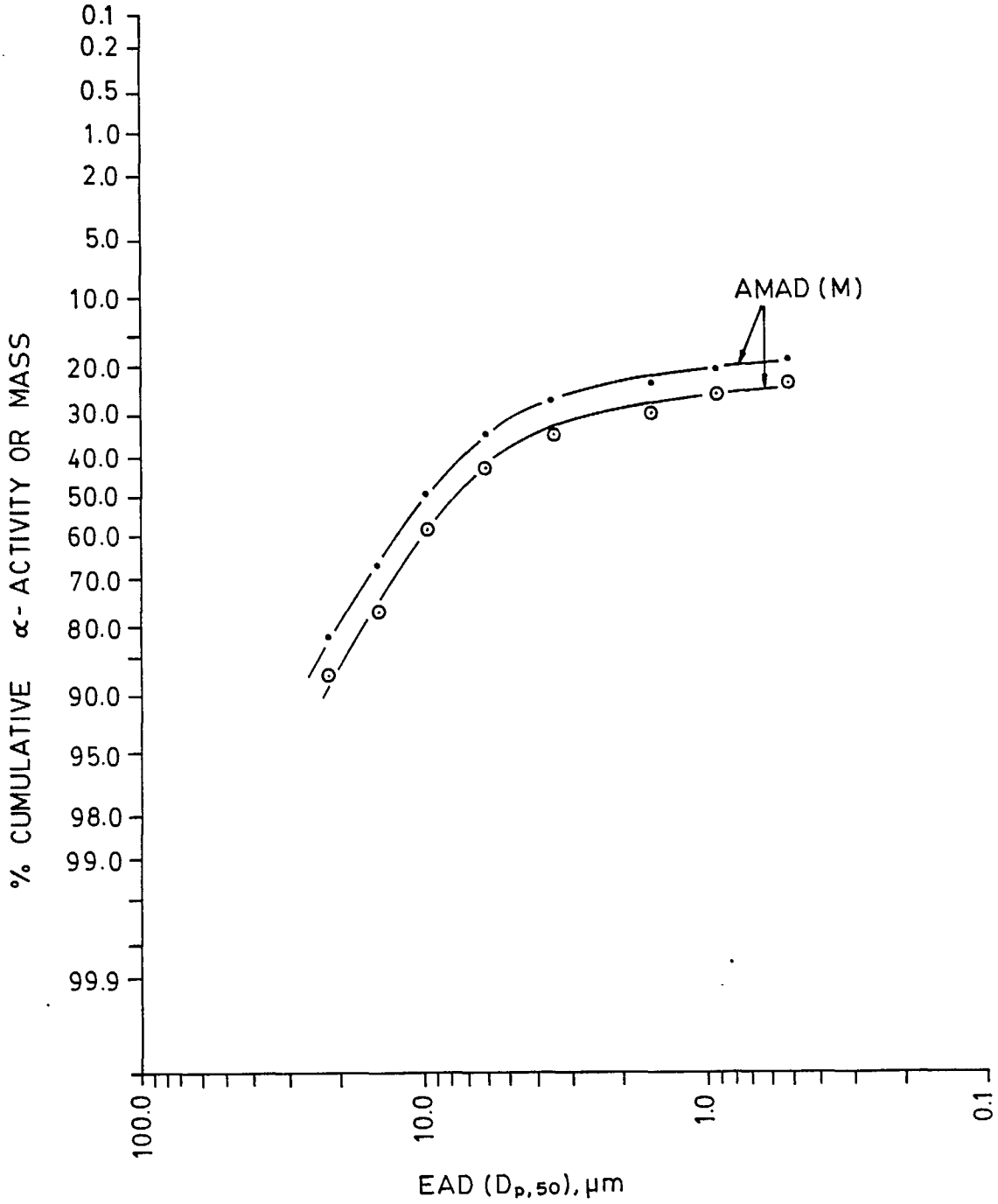

Fig. 16 - Percentage cumulative LLRD α-activity versus EAD for the grinding operation. (Note: the upper graph has been corrected for impactor stage efficiency. The lower graph shows non-corrected values.)

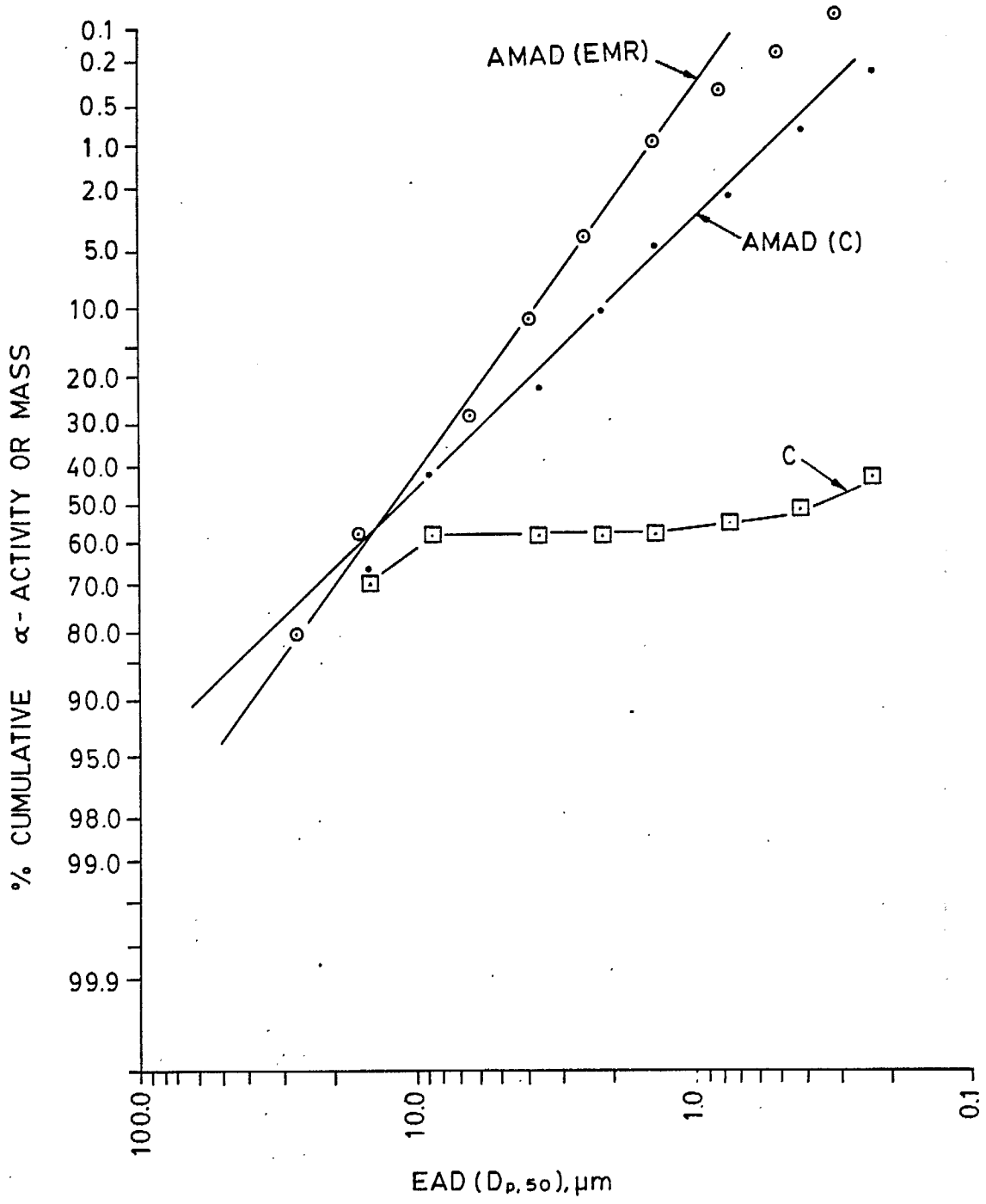

Fig. 17 - Percentage cumulative LLRD α-activity versus EAD for the yellowcake packaging operation.

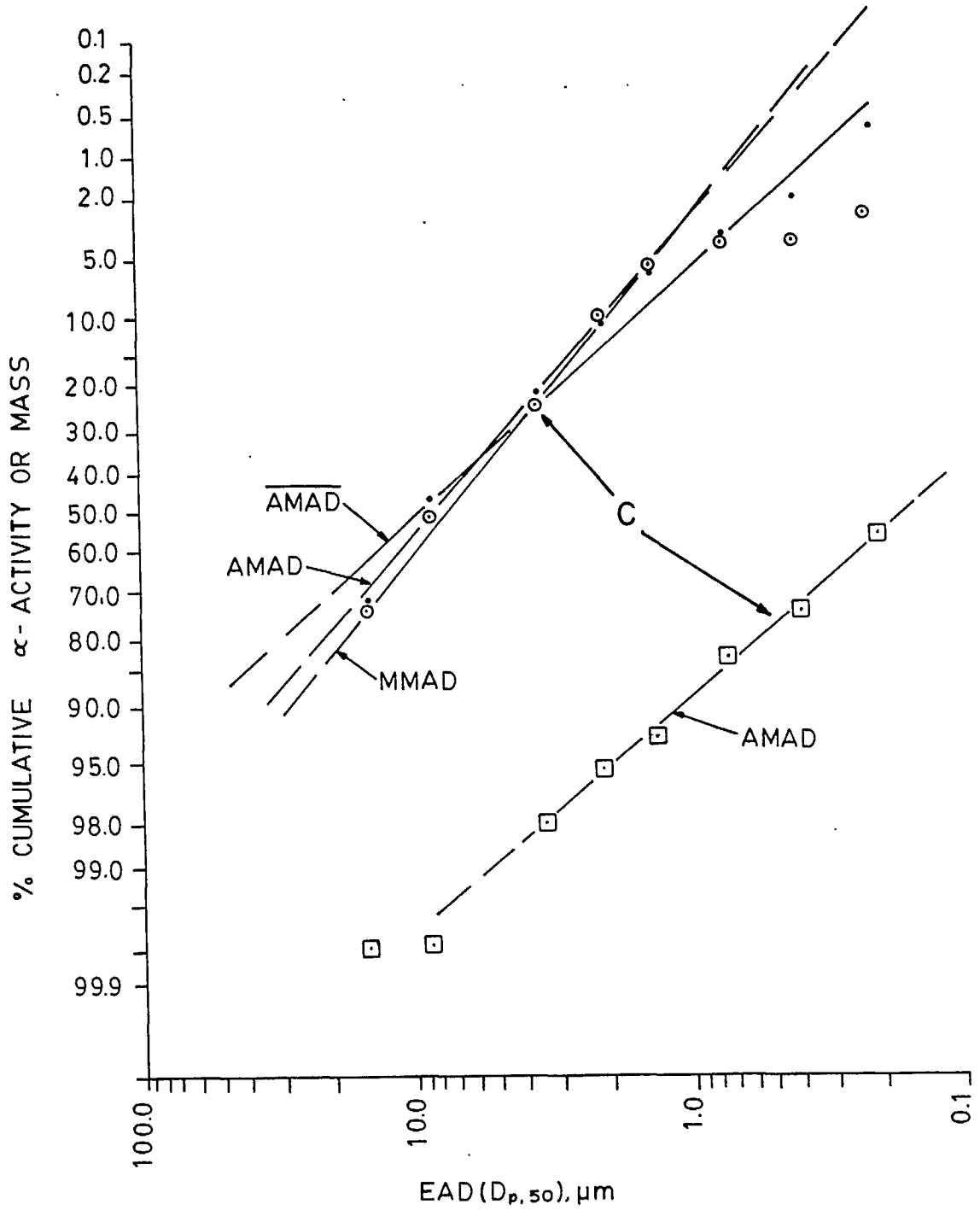

Fig. 18 - Percentage cumulative dust (MMAD), and percentage cumulative LLRD (AMAD), upper graphs, and radon progeny (lower graph) α-activity versus EAD for acid leaching.

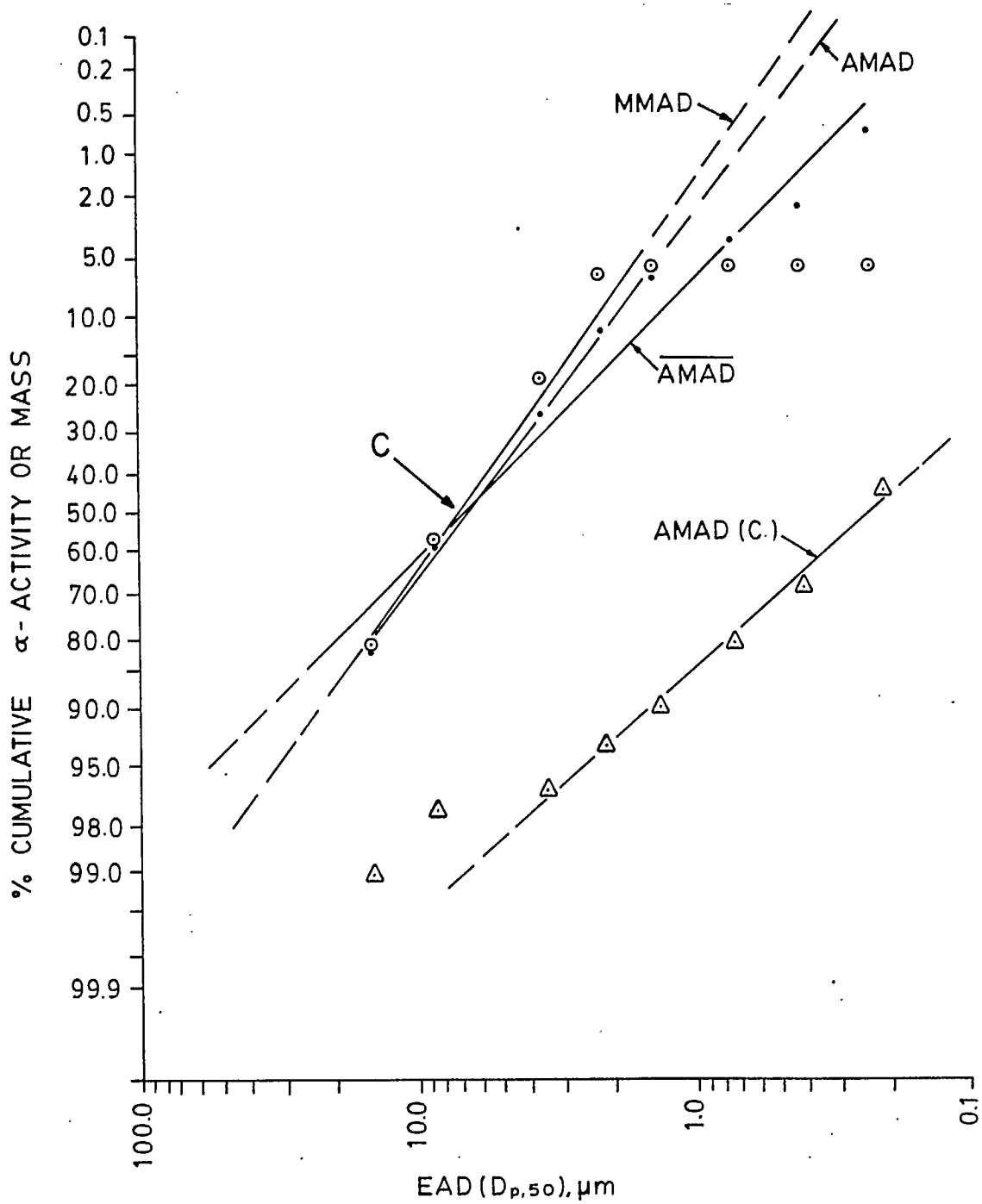

Fig. 19 - Percentage cumulative dust (MMAD), and percentage cumulative LLRD (AMAD), upper graphs, and radon progeny (lower graph) α-activity versus EAD for acid leaching.

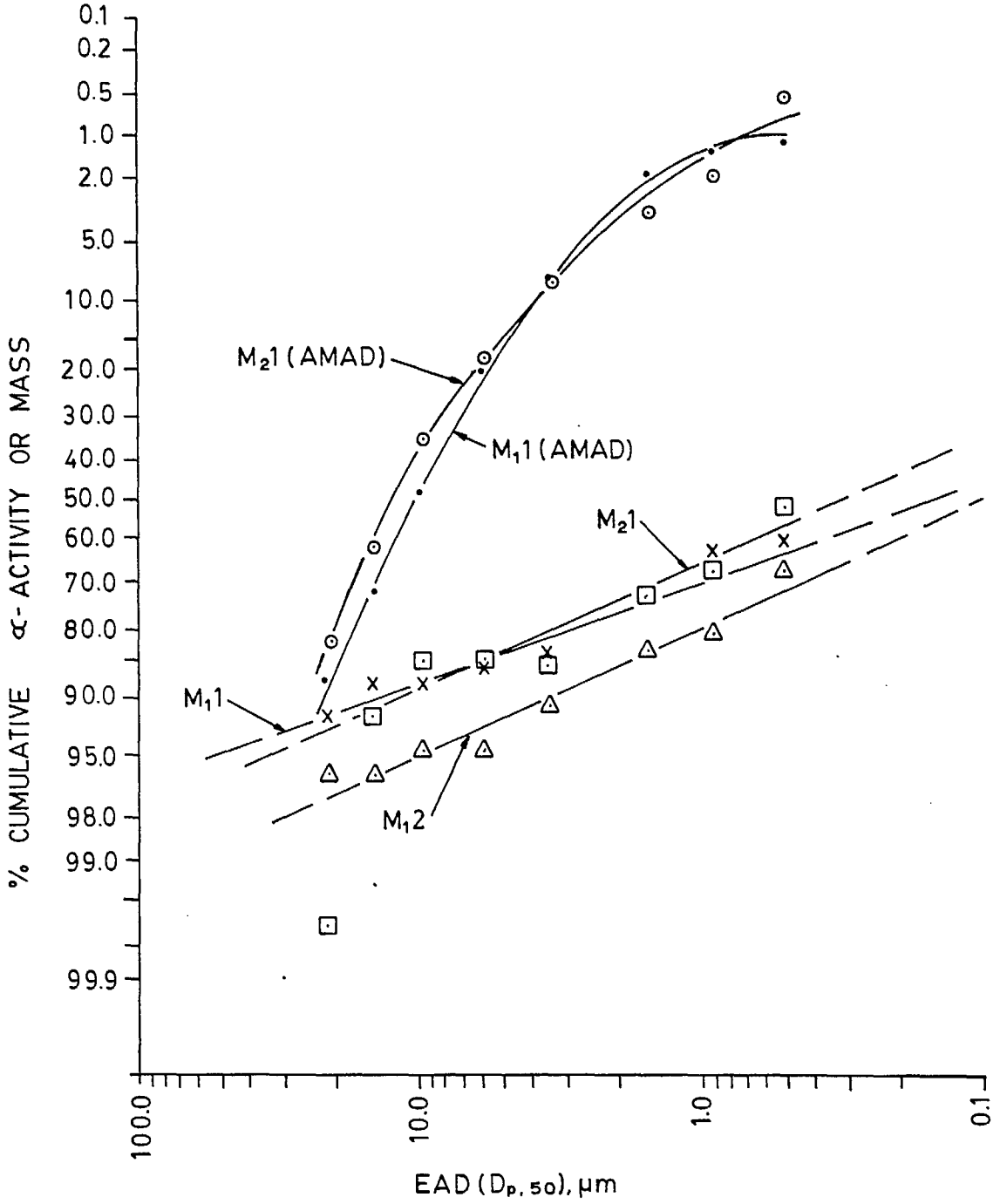

Fig. 20 - Percentage cumulative LLRD (upper graphs) and radon progeny (lower graphs) α-activity versus EAD for counter-current decantation operations. The numbers in M indicate the impactor and experimental run.

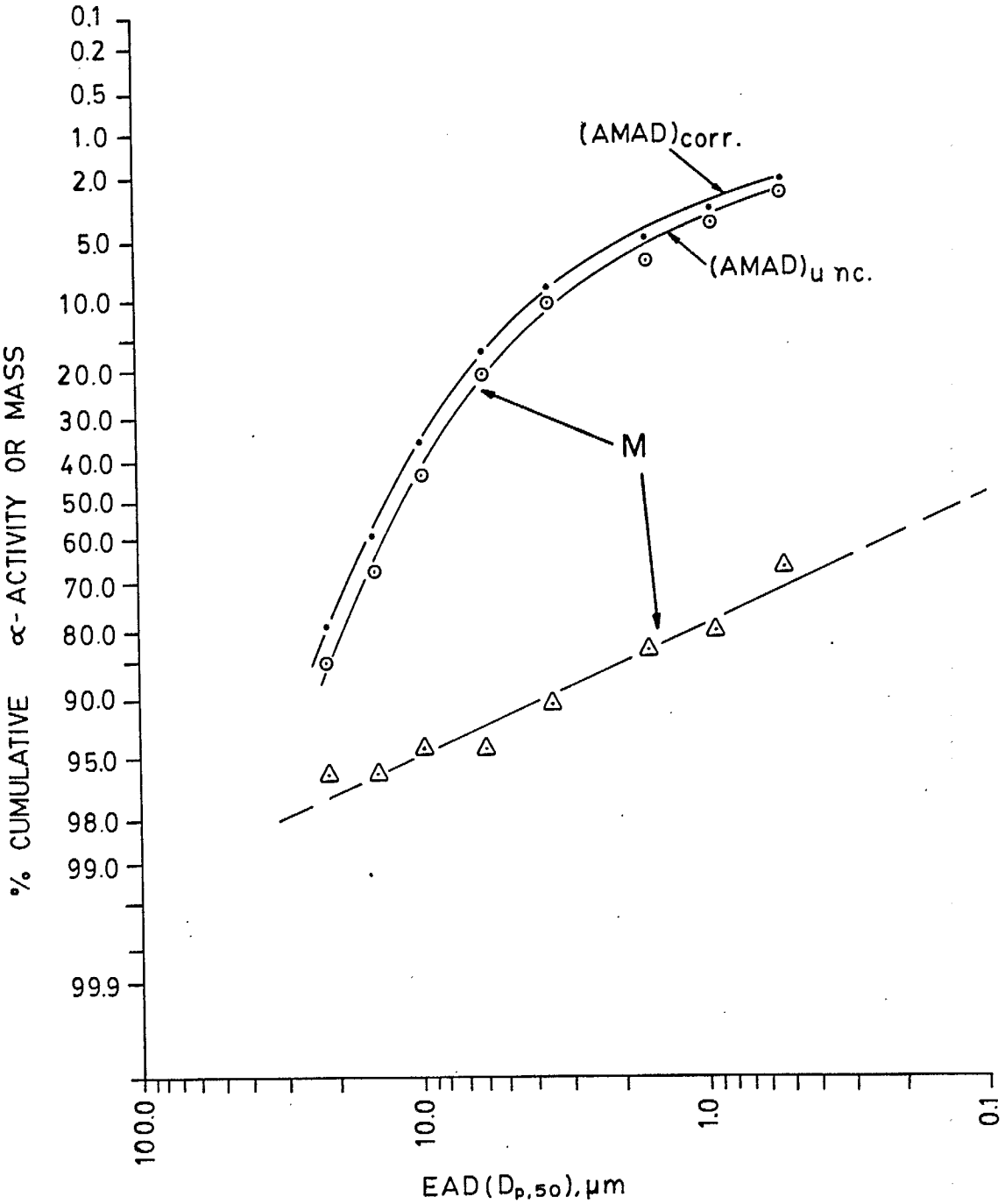

Fig. 21 - Percentage cumulative LLRD (upper graphs) and radon progeny (lower graph) α-activity versus EAD for counter-current decantation operations. (Note: the label corr. is used to indicate data corrected to take into account the collection efficiency of the different Marple impactor stages. Uncorrected data are indicated by the label unc.)

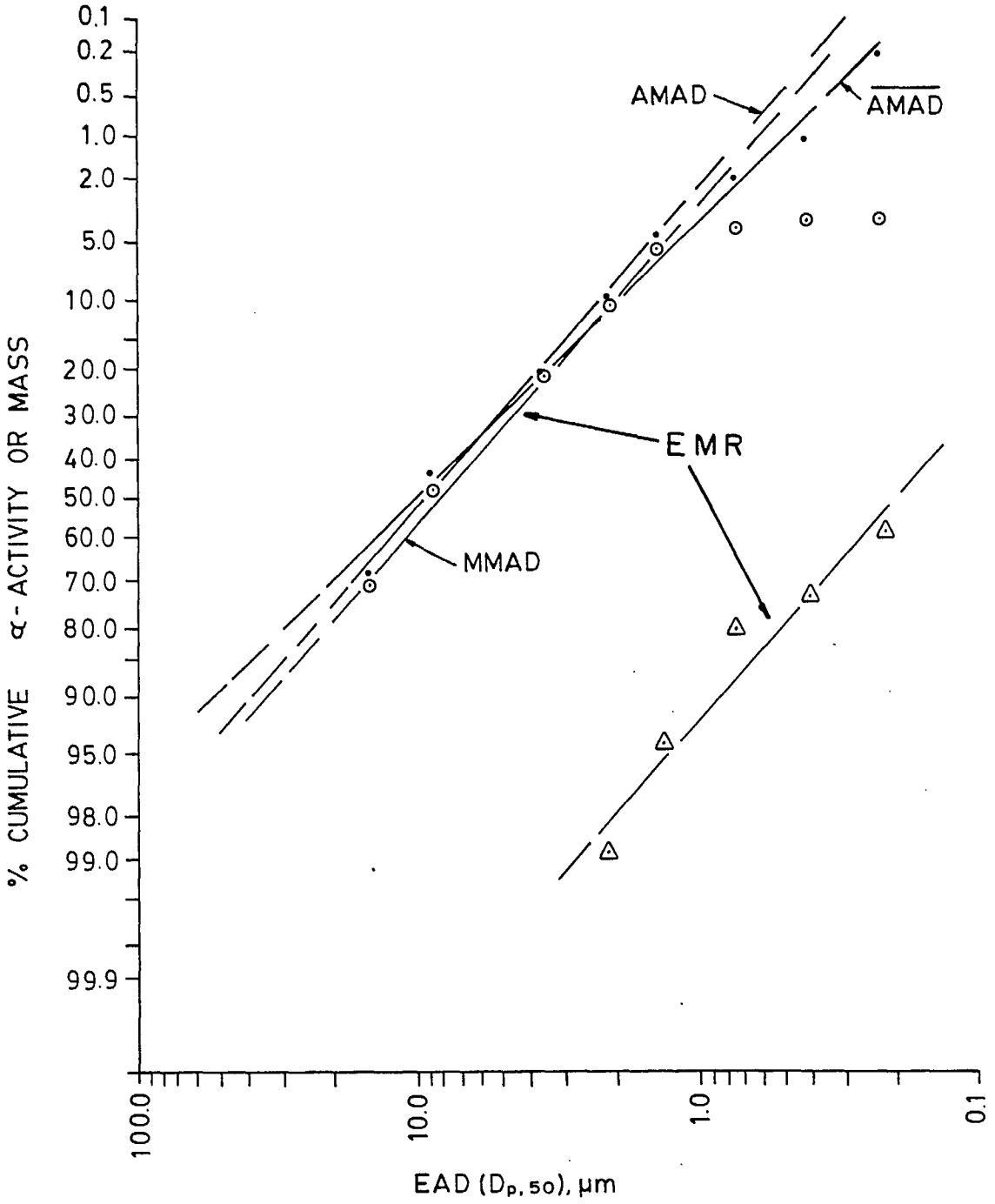

Fig. 22 - Percentage cumulative dust (MMAD), and percentage cumulative LLRD (AMAD), upper graphs, and radon progeny (lower graph) α-activity versus EAD for counter-current decantation operations.

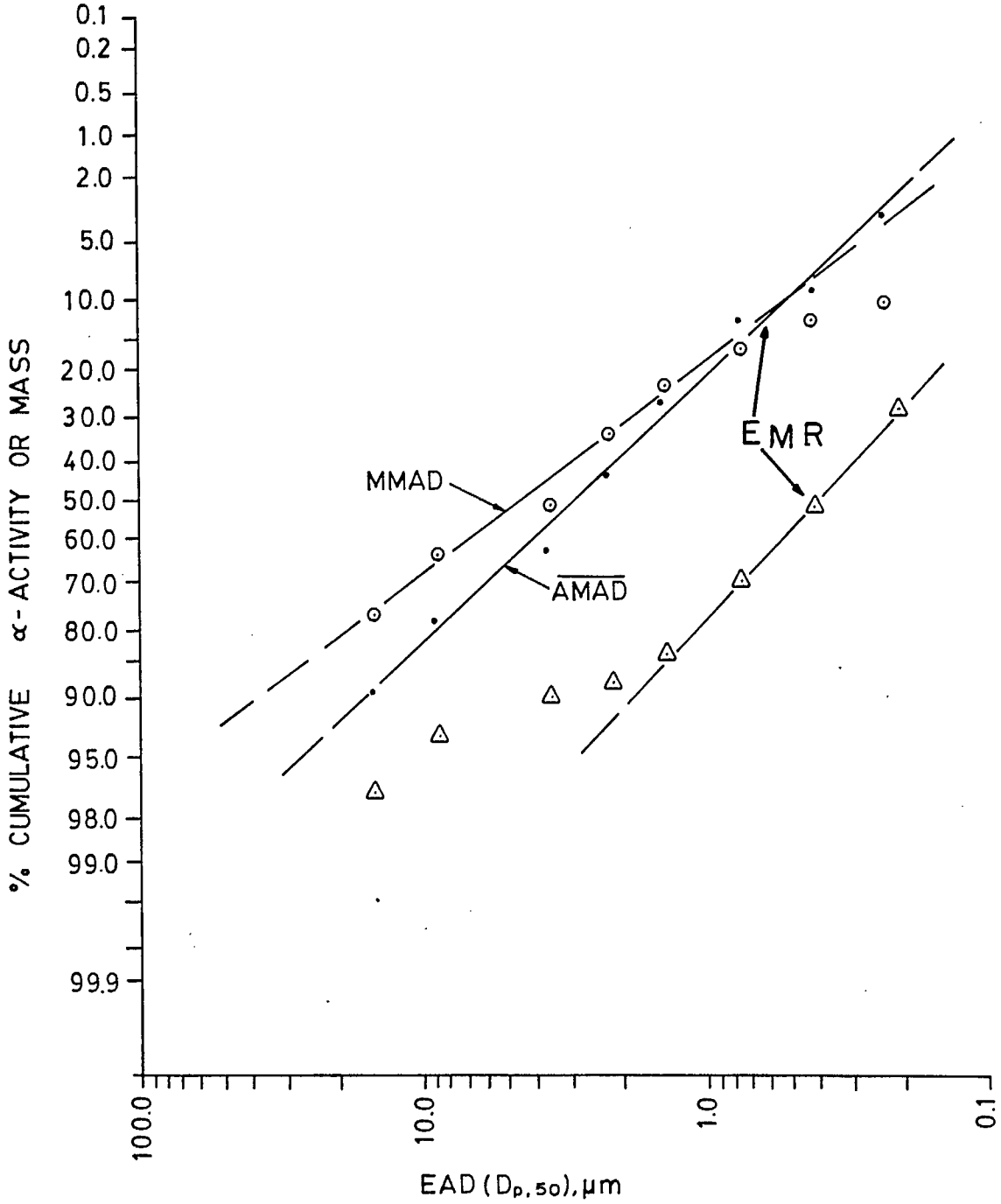

Fig. 23 - Percentage cumulative dust (MMAD) versus EAD, and percentage cumulative LLRD (AMAD) and radon progeny (lower graph) α-activity versus EAD for solvent extraction.

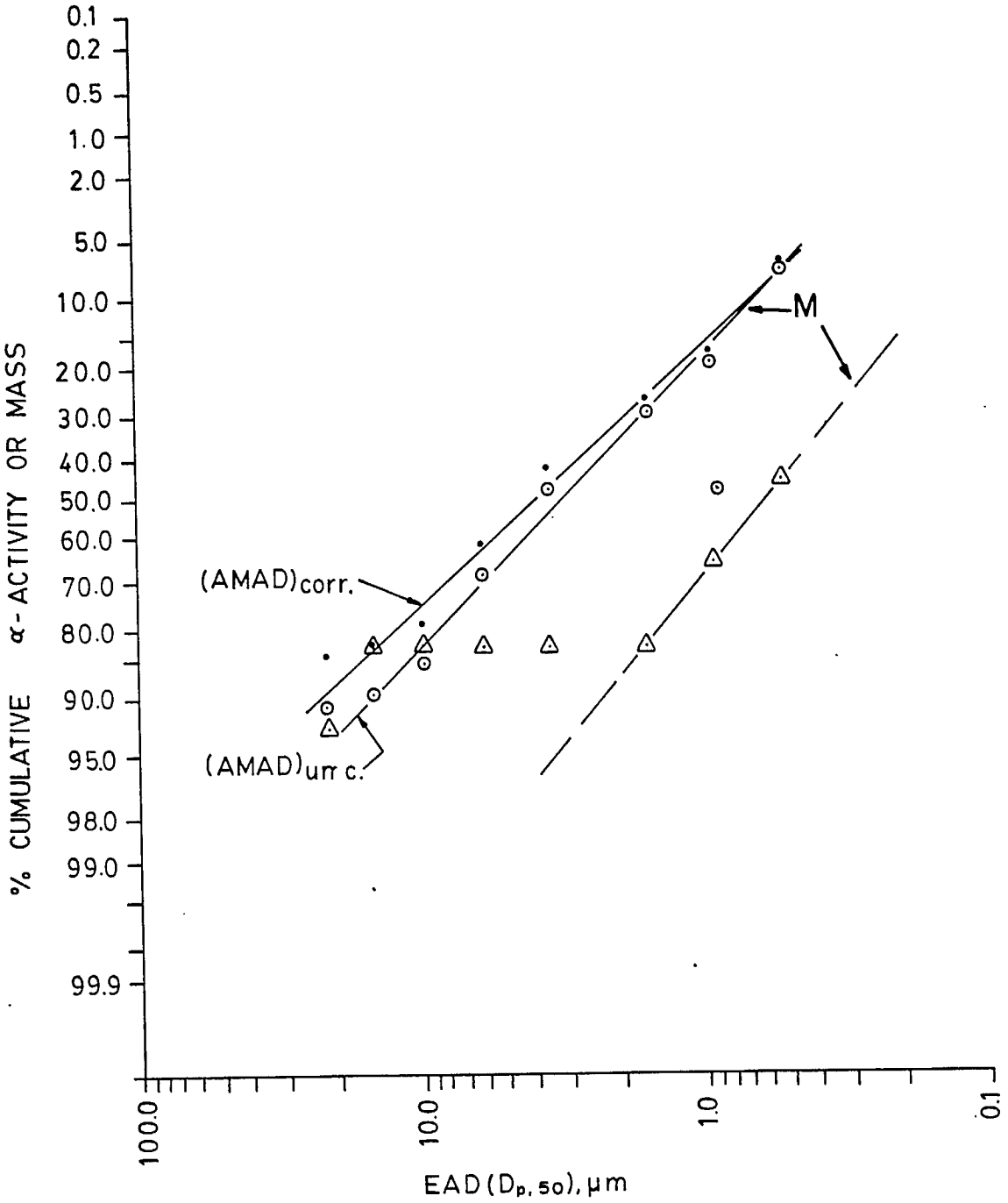

Fig. 24 - Percentage cumulative LLRD (upper graphs) and radon progeny (lower graph) α-activity versus EAD for solvent extraction. (Note: the label corr. is used to indicate data corrected to take into account the collection efficiency of the different Marple impactor stages. Uncorrected data are indicated by the label unc.)

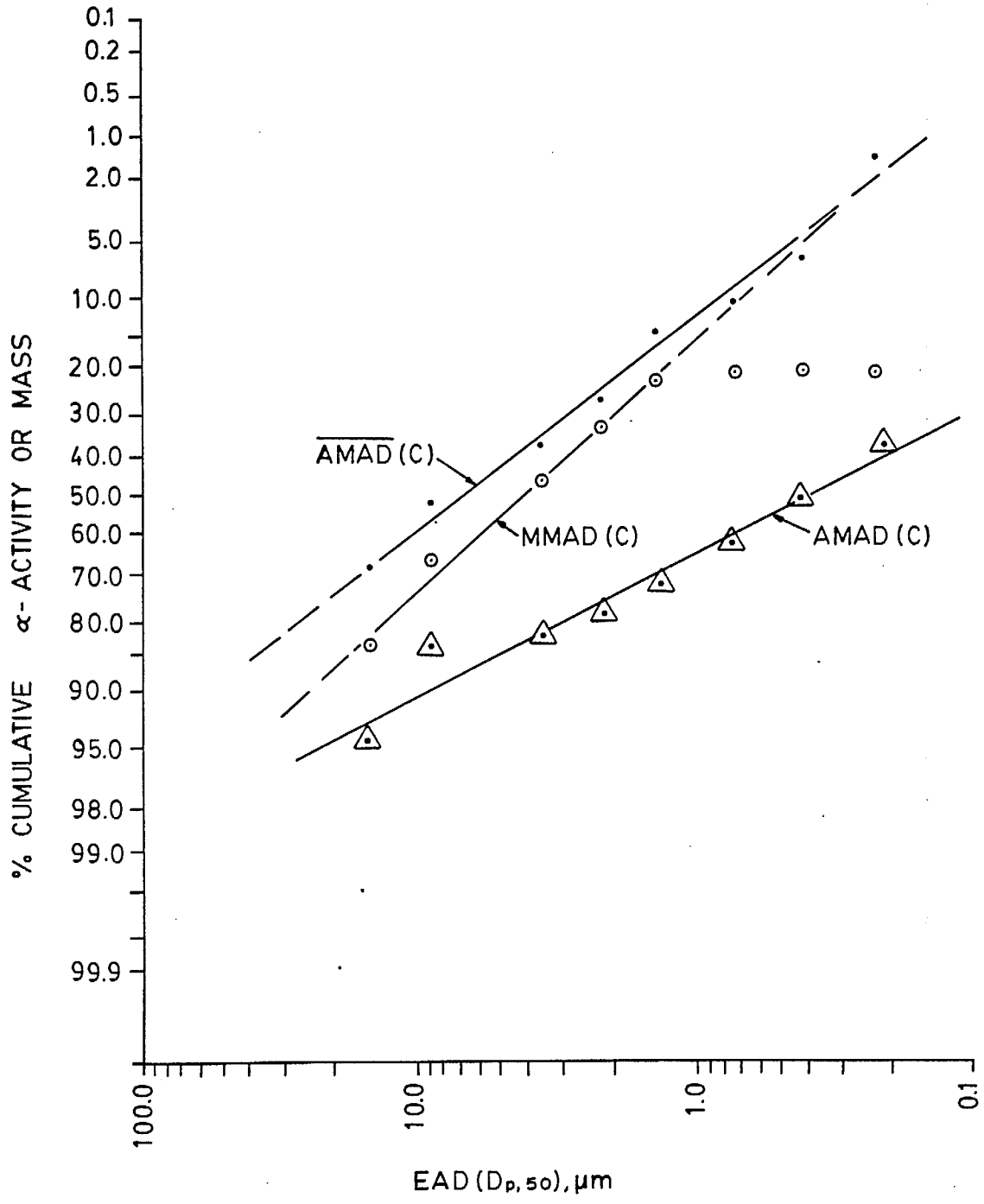

Fig. 25 - Percentage cumulative dust (MMAD) versus EAD, and percentage cumulative LLRD (AMAD), upper graph, and radon progeny (lower graph) α-activity versus EAD for yellowcake precipitation.

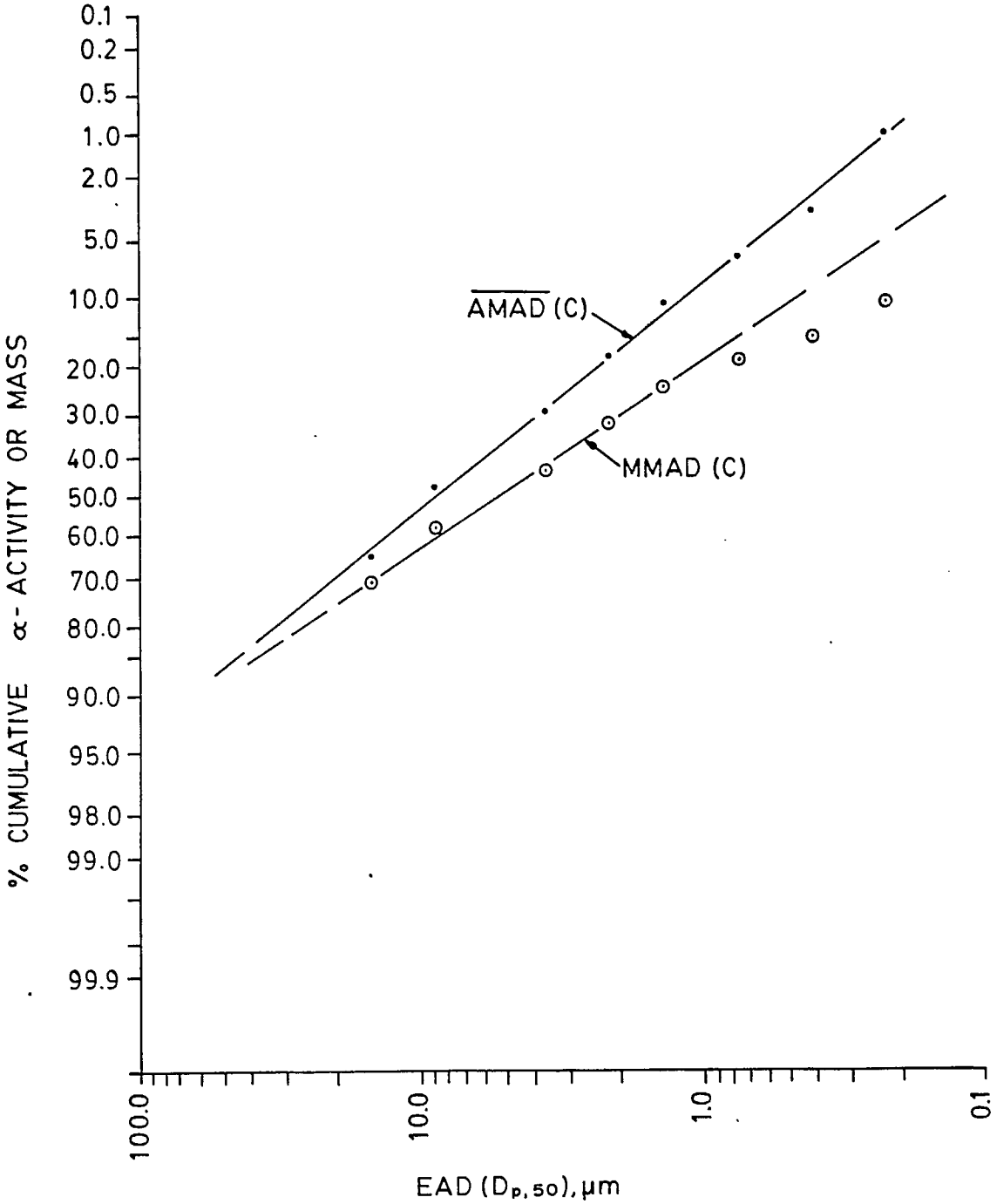

Fig. 26 - Percentage cumulative dust (MMAD) and LLRD (AMAD) α-activity versus EAD for yellowcake precipitation during the drying phase.

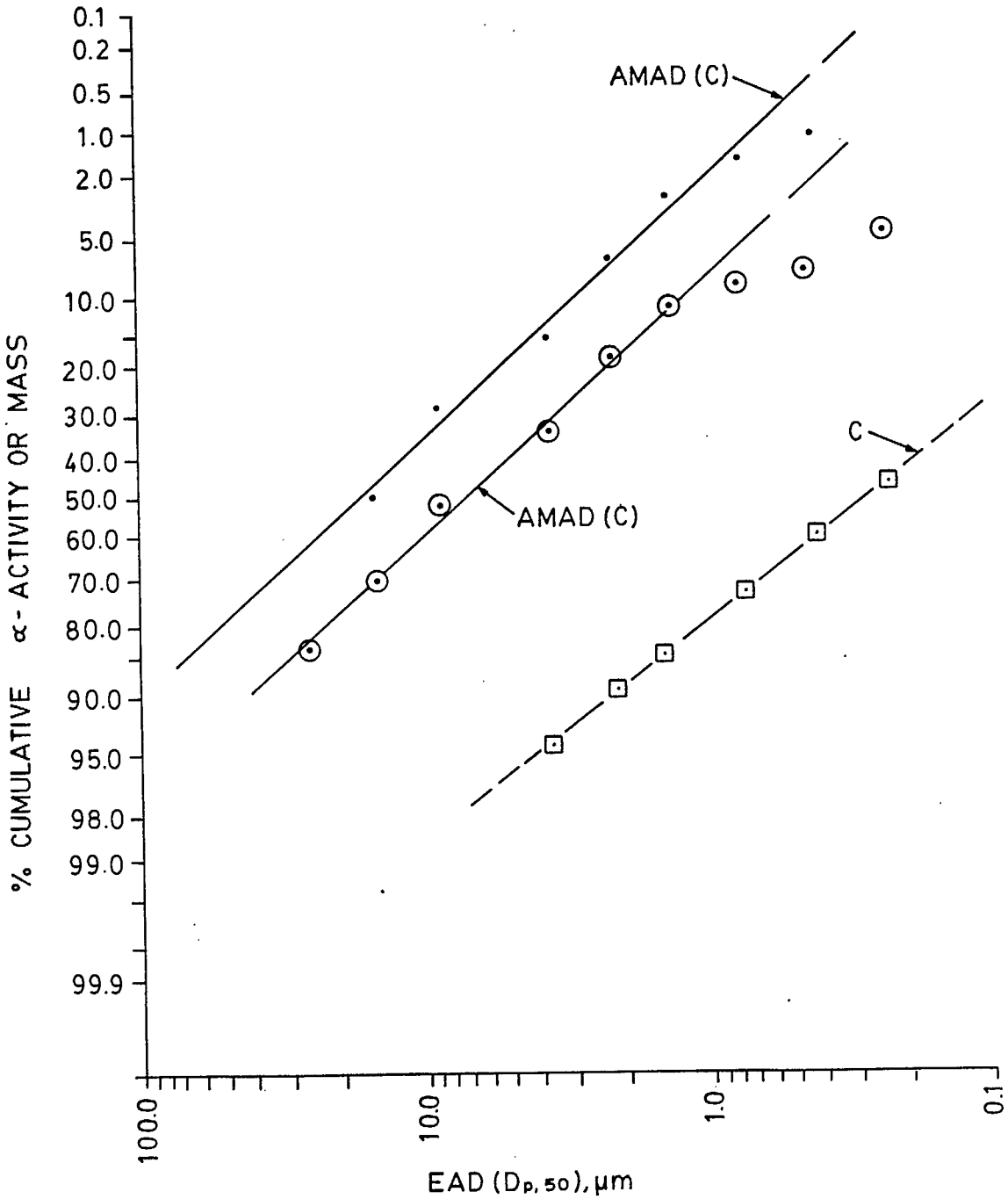

Fig. 27 - Percentage cumulative LLRD (upper graphs) and radon progeny (lower graph) α-activity versus EAD for yellowcake precipitation.

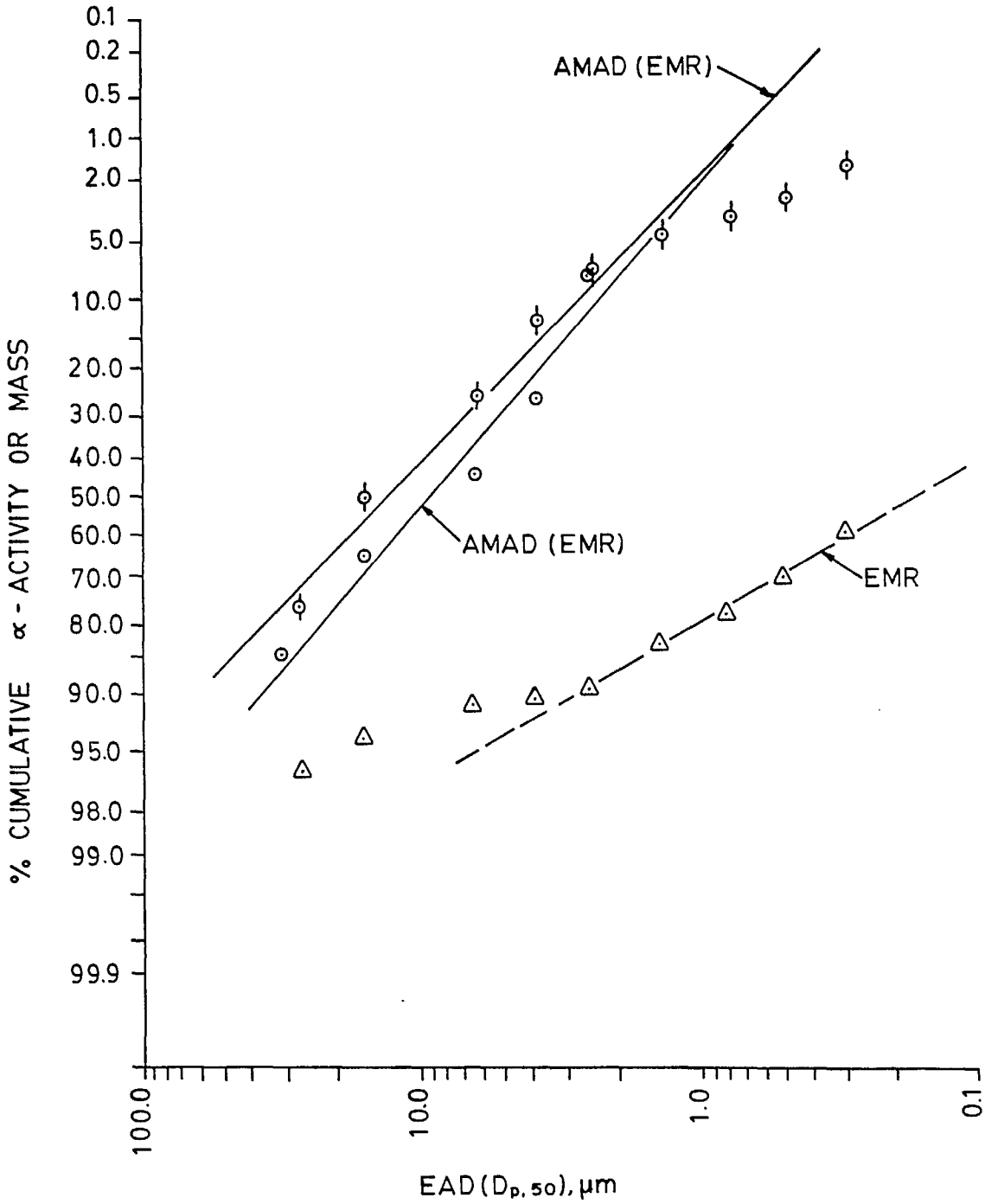

Fig. 28 - Percentage cumulative LLRD (upper graphs) and radon progeny (lower graph) α-activity versus EAD for yellowcake precipitation.

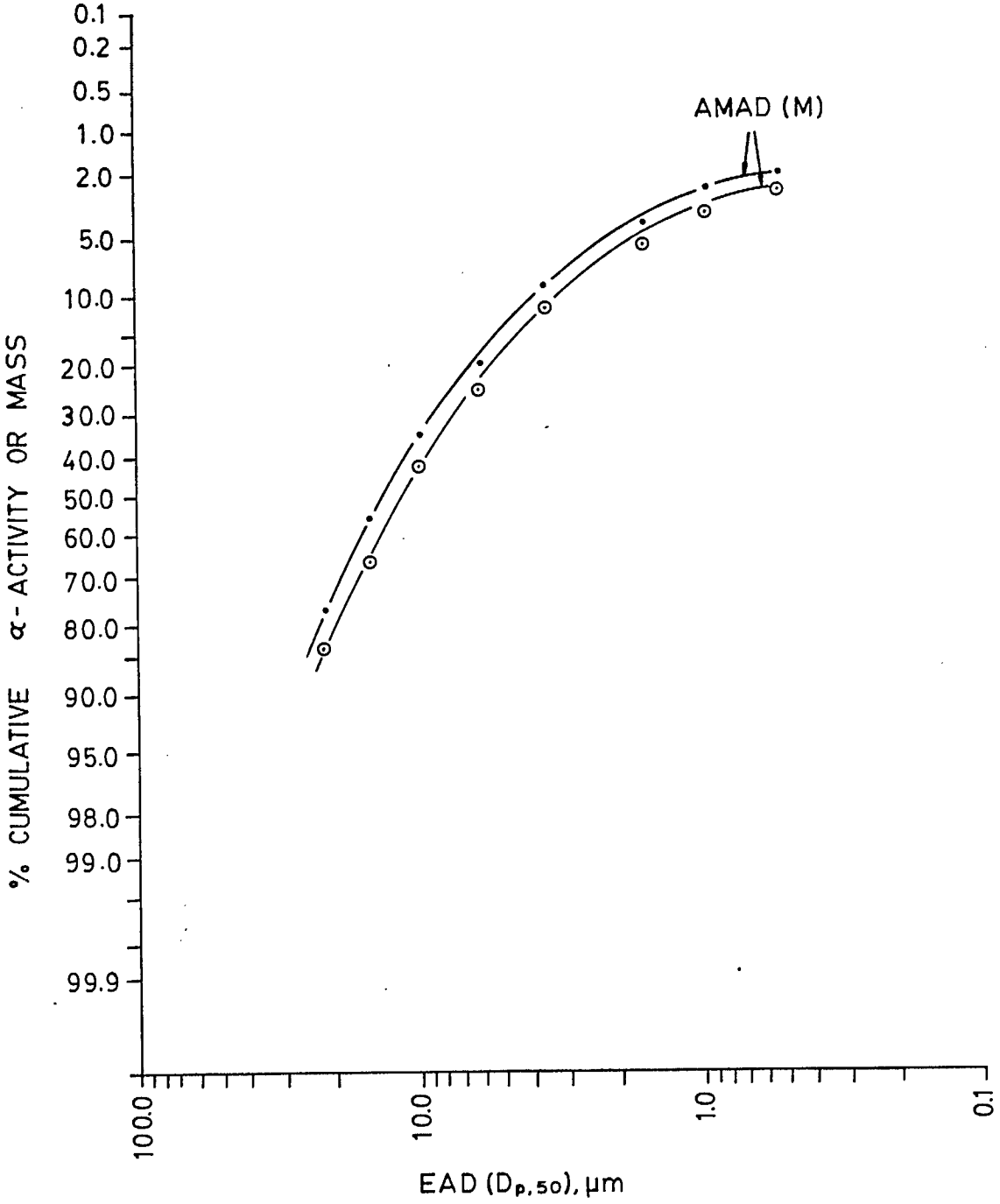

Fig. 29 - Percentage cumulative LLRD α-activity versus EAD for yellowcake precipitation. (Note: the upper graph has been corrected for impactor stage collection efficiency. The lower graph shows non-corrected values.)

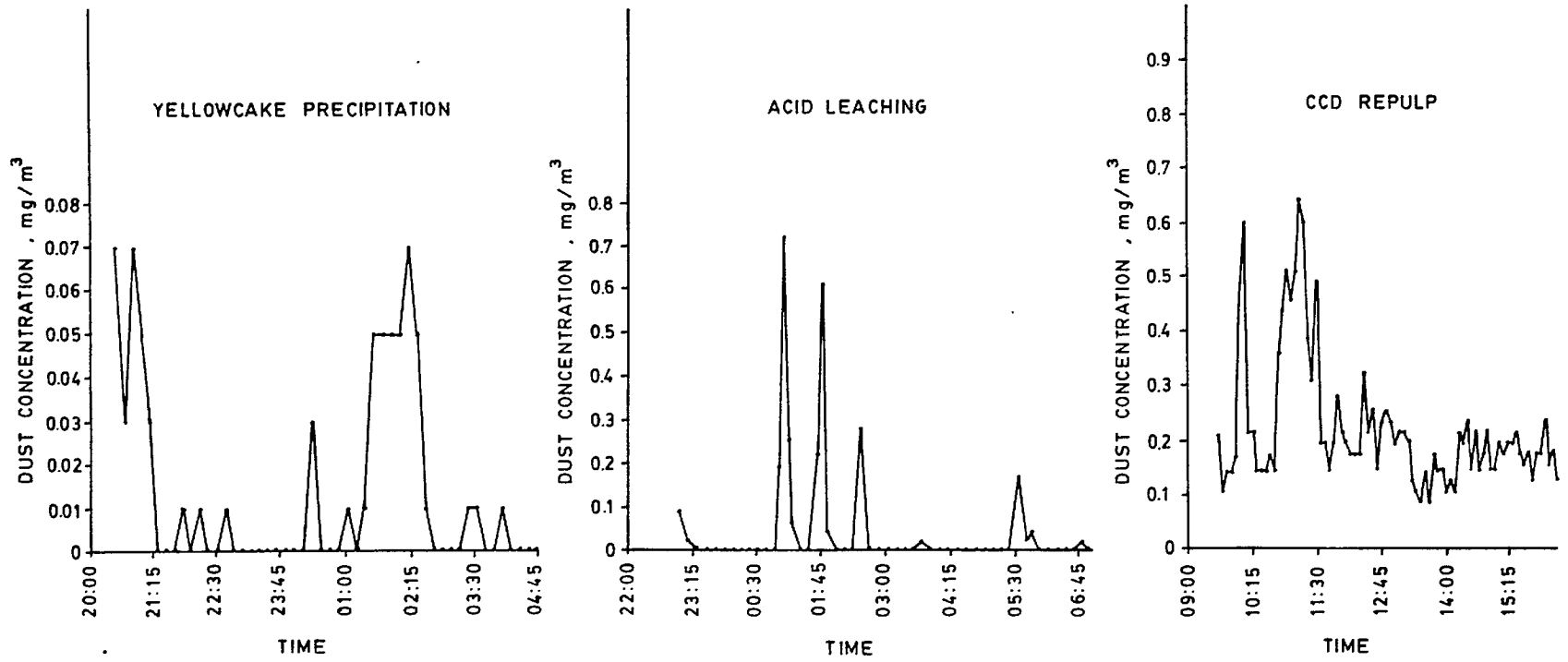

Fig 30 - Dust concentration for several physico-chemical operations.

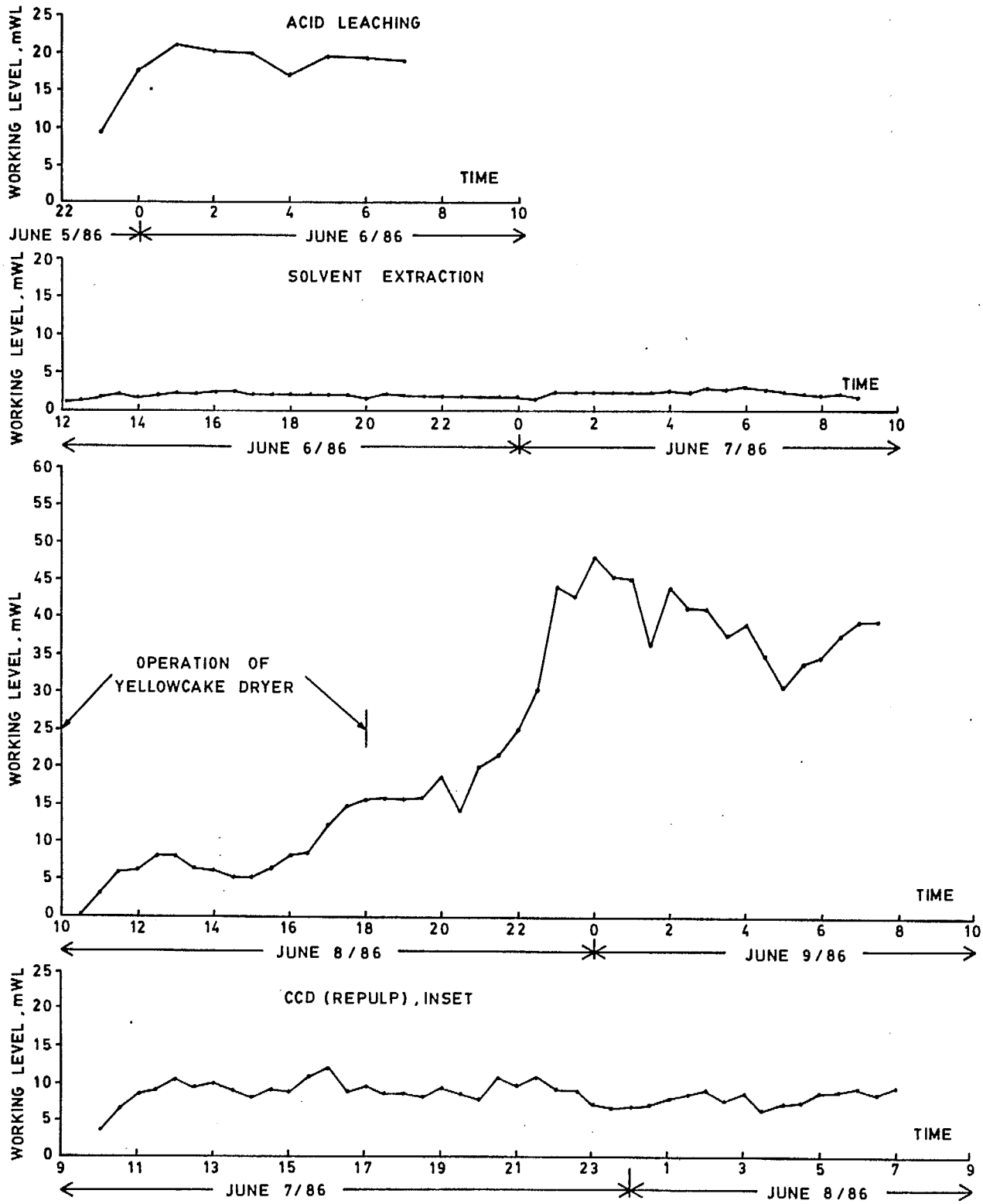

Fig. 31 - Radon progeny Working Level versus time for several physico-chemical operations.